Benthic contribution to seasonal silica budgets in two macrotidal estuaries in North-Western France

Mélanie Raimonet, Olivier Ragueneau, Karline Soetaert, Karima Khalil, Aude Leynaert, Emma Michaud, Brivaela Moriceau, Christophe Rabouille, Laurent Mémery

frontiers | Frontiers in Marine Science

TYPE Original Research
PUBLISHED 22 December 2023
DOI 10.3389/fmars.2023.1269142

OPEN ACCESS

EDITED BY
Eric 'Pieter Achterberg,
GEOMAR Helmholtz Center for Ocean Research Kiel, Germany

REVIEWED BY
Xiangbin Ran,
Ministry of Natural Resources, China
Shuijing Zhai,
Fujian Normal University, China

*CORRESPONDENCE
Mélanie Raimonet
melanie.raimonet@univ-brest.fr

RECEIVED 29 July 2023
ACCEPTED 20 November 2023
PUBLISHED 22 December 2023

CITATION
Raimonet M, Ragueneau O, Soetaert K, Khalil K, Leynaert A, Michaud E, Moriceau B, Rabouille C and Memery L (2023) Benthic contribution to seasonal silica budgets in two macrotidal estuaries in North-Western France. *Front. Mar. Sci.* 10:1269142. doi: 10.3389/fmars.2023.1269142

Benthic contribution to seasonal silica budgets in two macrotidal estuaries in North-Western France

Mélanie Raimonet [1,2]*, Olivier Ragueneau [1,2], Karline Soetaert [3], Karima Khalil [4], Aude Leynaert [1], Emma Michaud [1], Brivaela Moriceau [1], Christophe Rabouille [5] and Laurent Memery [1]

[1]CNRS, Univ Brest, IRD, Ifremer, LEMAR, IUEM, Plouzane, France, [2]LTSER, Zone Atelier Brest Iroise, Plouzane, France, [3]Department Estuarine and Delta Systems, Netherlands Institute for Sea Research, Yerseke, Netherlands, [4]Ecole Supérieure de Technologie d'Essaouira, Université Cadi Ayyad, Essaouira, Morocco, [5]Laboratoire des Sciences du Climat et de l'Environnement, UMR 1572, Gif sur Yvette, France

The paper aims to build seasonal silica budgets in two macrotidal estuaries, the Elorn and Aulne estuaries of the Bay of Brest (North-Western France), based on modeling and measurements, in order to increase our understanding of the silica (Si) cycle at land-sea interfaces. A diagenetic model was developed to quantify benthic Si fluxes, e.g. $aSiO_2$ deposition fluxes that are difficult to assess through direct measurements. Sediment cores were also seasonally sampled at six stations to provide data essential to parametrize and validate the model. Vertical profiles of porosity, burrowing depth, biodiffusive coefficients, concentrations of amorphous silica ($aSiO_2$) and silicic acid ($Si(OH)_4$ and the proportion of reactive $aSiO_2$ were measured. The results show that sites sampled along the Elorn and Aulne estuaries constitute significant net Si deposition areas (1-4.5 mmol Si m^{-2} d^{-1}), particularly in the upstream during winter and in midstream and downstream during summer. Year round, reprecipitation is negligible (< 3%) while burial accounts for the retention of ~ 30-80% of deposited $aSiO_2$. In winter, burial dominates the benthic Si budget. As surface-integrated benthic Si fluxes are low compared to riverine $aSiO_2$ fluxes, the Si export to coastal waters is high (93%) during winter. In contrast, in summer, burial accounts for 38% of river Si fluxes, and $Si(OH)_4$ flux from the sediment is high as a result of enhanced benthic recycling and bioirrigation. Internal estuarine processes, e.g., benthic and pelagic primary production, dissolution and benthic Si fluxes, surpass river fluxes in magnitude during summer. Overall, we conclude that the Elorn and Aulne macrotidal estuaries are efficient filters of Si, retaining about 4-38% of river Si fluxes, and even 6-67% when accounting for retention in intertidal marshes, but with massive exports occurring during winter floods.

KEYWORDS

silica cycle, estuary, diagenetic modeling, bioturbation, benthic-pelagic coupling

1 Introduction

In aquatic ecosystems, silicon (Si) is an essential element for the growth of diatoms, which account for up to 75% of the coastal primary production (Nelson et al., 1995) and which play an essential role in the oceanic carbon biological pump (Buesseler, 1998; Ragueneau et al., 2006; Tréguer et al., 2018). The inputs of reactive Si to coastal and oceanic waters are mainly transported by rivers (Tréguer et al., 2021), essentially in the dissolved form, i.e. silicic acid $Si(OH)_4$ (Dürr et al., 2011), but with a non-negligible contribution in particulate form, i.e. amorphous silica ($aSiO_2$), as phytoliths and products of riverine primary production (Conley, 1997; Farmer et al., 2005). These inputs are mostly natural but, in the last few decades, anthropogenic activities leading to eutrophication (Conley et al., 1993; Garnier et al., 2021), river damming (Humborg et al., 1997; Maavara et al., 2020) or the proliferation of invasive species related to globalization of maritime transport (Ragueneau et al., 2005a) have strongly disturbed the transit of Si from land to coastal waters, most often decreasing it strongly. The synergistic decrease of Si river loads and the enhanced nitrogen and phosphorus run-off due to agriculture, industry and urbanization, have decreased the ratios of Si over nitrogen and phosphorus in coastal waters (Garnier et al., 2010; Maavara et al., 2020). This has led to Si limitation of primary production and shifts from diatom to dinoflagellate-dominated phytoplankton communities that are potentially toxic to consumers, in many coastal ecosystems around the world (Officer and Ryther, 1980; Garnier et al., 2010), and could be associated with an increase in diatom toxicity (e.g. *Pseudo-nitzschia fraudulenta*; Tatters et al., 2012).

At the land-sea interface, estuaries constitute potentially efficient filters for nitrogen (~22%), phosphorus (~24%) and carbon (~60%) (Laruelle, 2009; Regnier et al., 2013). While data are quite abundant for nitrogen or phosphorus, datasets for Si are very sparse or based on punctual field work (Ragueneau et al., 2010; Dürr et al., 2011; Mangalaa et al., 2017), despite the importance of this element for coastal and oceanic ecological and biogeochemical processes, tightly coupled to the carbon cycle through silicified organisms e.g. diatoms, plants, sponges, radiolarians (Tréguer, 2002; Tréguer et al., 2021). Estuaries are characterized by high primary production often dominated by diatoms (Ragueneau et al., 2002b; Roubeix et al., 2008b; Wallington et al., 2023), and high $aSiO_2$ dissolution resulting from high bacterial biomass and increased salinity (Roubeix et al., 2008a; Loucaides et al., 2010). The distribution of diatom production and degradation in estuarine waters emerges by a complex balance between light and nutrients for production (DeMaster et al., 1983; Zhang et al., 2020) and between temperature, salinity, and bacterial activity for degradation (Ragueneau et al., 2002b; Roubeix et al., 2008a). However the estuarine filter capacity is strongly linked to the benthic ecosystem through $aSiO_2$ deposition, recycling and/or storage (Carbonnel et al., 2009; Rebreanu, 2009) and through $Si(OH)_4$ reprecipitation (Michalopoulos and Aller, 2004; Ehlert et al., 2016). Finally, tidal saltmarshes can constitute transient sources of $Si(OH)_4$, especially during summer (Struyf et al., 2006) and increase the residence time of Si in estuaries (Carey and Fulweiler, 2014).

Although the benthic Si cycle is often neglected in estuaries because of lower benthic fluxes than river fluxes (Arndt et al., 2009), benthic Si fluxes can become significant, especially during summer, due to the reduced river discharges (Anderson, 1986), higher dissolution rates (Yamada and D'Elia, 1984; Rebreanu, 2009) or enhanced bioirrigation activities (Green et al., 2004). Especially during summer, benthic $Si(OH)_4$ fluxes can slightly enhance (Arndt and Regnier, 2007) or even sustain pelagic primary production (Ragueneau et al., 2002a). The interactions between benthic and pelagic ecosystems are even stronger along estuaries because of water column shallowness (Sundbäck et al., 2003), resuspension processes induced by a strong hydrodynamic regime from tidal to seasonal scales (Gehlen and Van Raaphorst, 2002; Welsby et al., 2016), lateral loads from large intertidal areas (Sun et al., 1994; Struyf et al., 2006; Wallington et al., 2023), and climate change (Fulweiler and Nixon, 2009) or the presence of benthic suspension feeders (Cloern, 1982; Ragueneau et al., 2002a).

Estuaries are indeed highly dynamic and complex zones submitted to intense and interacting physical, biological and biogeochemical processes leading to strong spatial and temporal gradients at various scales e.g. upstream-downstream gradient, cross-section, vertical, tidal or seasonal variations (Pritchard, 1967; Cloern et al., 2017), and modified by anthropogenic activities (Nichols et al., 1986). Studying estuaries requires modeling and/or large datasets to document these gradients. Different approaches have been used to build Si budgets and estimate the filtering and retention capacities of aquatic systems from rivers to coastal waters (Ragueneau et al., 2005a; Soetaert et al., 2006; Arndt et al., 2009; Laruelle, 2009; Wallington et al., 2023). The most common methods are mixing diagrams, box models, or dynamic reactive-transport models of the pelagic ecosystem (Peterson, 1979; Anderson, 1986; Soetaert et al., 2006; Arndt et al., 2007; Testa and Kemp, 2008; Arndt et al., 2009; Carbonnel et al., 2009). Mixing diagrams are useful for determining the gains and losses along salinity gradients, assuming a steady state river flow (Anderson, 1986; Ragueneau et al., 2002b). Contrary to mixing diagrams, box models account for internal estuarine processes (Ragueneau et al., 2005a; Carbonnel et al., 2009). Reactive-transport models are useful for representing coupled physical and biological processes with strong spatial and temporal variations (Arndt and Regnier, 2007), and for highlighting the potentially erroneous interpretations that may result from mixing diagrams when transient river flows are not considered (Regnier et al., 1998; Arndt et al., 2009).

In general, estimates of benthic retention are performed through indirect methods by determining differences between pelagic input and output fluxes (Carbonnel et al., 2009), by subtracting benthic fluxes (Ragueneau et al., 2005a), or through analytical modeling (Arndt and Regnier, 2007): however, such estimates neglect or simplify the vertical discretization of benthic fluxes, and do not take into account the non-local bioirrigation processes. Even if calibration and data from the literature is often used to calibrate and/or validate models, the acquisition of extensive datasets is essential to better constrain the model and reduce uncertainties. If the quantification of $Si(OH)_4$ and $aSiO_2$ contents is an essential requirement, better constraints could be obtained by

10.3389/fmars.2023.1269142

complementary experiments on major processes in order to quantify the seasonality of pelagic $aSiO_2$ production, the proportion of highly reactive $aSiO_2$, or bioturbation coefficients.

The aim of this study is to investigate the seasonality of the main processes involved in the benthic Si cycle along the estuaries of the two main rivers (Elorn, Aulne) that extend to the Bay of Brest. The methodology involves diagenetic modeling coupled to measurements. After the seasonal characterization of deposition fluxes along the estuaries, the main processes (e.g. diffusion fluxes at the sediment-water interface, bioirrigation, reprecipitation, burial) involved in the benthic Si cycle of estuarine muddy sediments are quantified. Finally, the retention of Si through benthic estuarine processes is estimated and compared to river fluxes and pelagic processes (e.g. production).

2 Material and methods

2.1 Model description

The diagenetic Si model was modified from Khalil et al. (2007) and implemented in the R software (http://cran.r-project.org). A short description of equations, processes and parameters is given below.

The general equation of the reactive-transport model affecting solids and solutes (Eq. 1) represent diffusive and advective transport (first and second terms, respectively) and reactive processes (third term):

$$\frac{\partial \xi C_i}{\partial t} = -\frac{\partial}{\partial z}\left(-\xi D \frac{\partial C_i}{\partial z}\right) - \frac{\partial}{\partial z}(\xi w C_i) + \Sigma \xi R \quad (1)$$

All fluxes are in mmol m^{-3} d^{-1} and are detailed below.

The originality of the work of Khalil et al. (2007) is to implement two variables of $aSiO_2$ with different reactivity. The model has thus three sets of variables: less reactive $aSiO_2$ concentrations (C_{aSiS}, µmol l^{-1}), highly reactive $aSiO_2$ concentrations (C_{aSiF}, µmol l^{-1}) and dissolved $Si(OH)_4$ concentrations (C_{dSi}, µmol l^{-1}) implemented in Eqs. 2, 3, 4 and 5.

The transport of the two solid fractions - less and highly reactive $aSiO_2$ - is controlled by the biodiffusion rates (D_b, m^2 d^{-1}) linked to sediment mixing by benthic organisms, and by the advection rates (w, m d^{-1}) linked to the accumulation of newly deposited particles and steady-state compaction.

$$\frac{\partial (1-\phi) C_{aSiS}}{\partial t} = -\frac{\partial}{\partial z}\left(-(1-\phi) D_b \frac{\partial C_{aSiS}}{\partial z} + w(1-\phi) C_{aSiS}\right) - (1-\phi) R_{dissS} \quad (2)$$

$$\frac{\partial (1-\phi) C_{aSiF}}{\partial t} = -\frac{\partial}{\partial z}\left(-(1-\phi) D_b \frac{\partial C_{aSiF}}{\partial z} + w(1-\phi) C_{aSiF}\right) - (1-\phi) R_{dissF} \quad (3)$$

The biodiffusion rate is depth-dependent and calculated at each depth as follows:

$$For\ z \le z_b,\ D_b(z) = D_{b0}$$

$$For\ z > z_b,\ D_b(z) = D_{b0} exp(-(z - z_b) \times coeff_b)$$

where D_{b0} is the surface biodiffusion coefficient (m^2 d^{-1}), z_b is the biodiffusion depth for solids (m) and $coeff_b$ is the exponential decrease constant for biodiffusion (m).

The $aSiO_2$ dissolution term (R_{dissS} or R_{dissF}; Eqs. 4 and 5) is parametrized by different dissolution rates (k_{aSiS} and k_{aSiF}, d^{-1}, dependent on *in situ* temperature and salinity) and equilibrium concentrations (C_{dSieqS} and C_{dSieqF}, µmol l^{-1}) for each $aSiO_2$ phase.

$$R_{dissS} = k_{aSiS}\ C_{aSiS}\left(1 - \frac{C_{dSi}}{C_{dSieqS}}\right) \quad (4)$$

$$R_{dissF} = k_{aSiF}\ C_{aSiF}\left(1 - \frac{C_{dSi}}{C_{dSieqF}}\right) \quad (5)$$

Note that the porosity ϕ is depth-dependent and defined at each depth as follows:

$$\phi(z) = (\phi_0 - \phi_\infty) \exp(-z \times coef_\phi) + \phi_\infty$$

Where ϕ_0 is the porosity at sediment-water interface, ϕ_∞ the asymptotic porosity and z_{por} the exponential decrease constant for porosity.

The reactive-transport of solutes - $Si(OH)_4$ (noted dSi in equations) - is modified from Khalil et al. (2007) and described in Eq. 6. Advection is neglected because of the dominance of the diffusive process (Peclet number >> 1; McManus et al., 1995). The processes of molecular diffusion, dissolution ($R_{diss} = R_{dissF} + R_{dissS}$) and reprecipitation ($R_{precip} = K_p\ (C_{dSi} - C_{dSieqp})$) are kept as described by Khalil et al. (2007). Secondly, a bioirrigation process (R_{irr}) is added to take into account the transport of $Si(OH)_4$ with solutes by bioturbation activities.

$$\frac{\partial \phi C_{dSi}}{\partial t} = -\frac{\partial}{\partial z}\left(-\phi D_{dSi} \frac{\partial C_{dSi}}{\partial z}\right) + \phi R_{diss} - \phi R_{precip} - \phi R_{irr} \quad (6)$$

Bioirrigation is represented with a non-local term described in Eq. 7 for depth $z \le z_{irr}$ (Emerson et al., 1984; Boudreau, 1994).

$$R_{irr} = \alpha\ (C_{dSi} - C_{dSi0}) \quad (7)$$

The bioirrigation rate parameter α (d^{-1}) is constant over the bioirrigation depth (m) and exponentially decreases below that depth. C_{dSi0} is the concentration of $Si(OH)_4$ at the sediment-water interface (z=0).

At the sediment-water interface (z=0), diffusive fluxes of $Si(OH)_4$ are prescribed by Fick's first law of diffusion (Eq. 8).

$$F_{dSi0} = -\phi_0\ D_{dSi0} \frac{\partial C_{dSi}}{\partial z} \quad (8)$$

Where D_{dSi0} is the diffusion coefficient for $Si(OH)_4$ (m^2 d^{-1}) and $\frac{\partial C_{dSi}}{\partial z}$ is the concentration gradient of $Si(OH)_4$ (mmol m^{-3} m^{-1}) at sediment-water interface.

The upper boundary of the solid fraction is prescribed as a net deposition flux (including resuspension and benthic primary production). At the lower boundary, zero-gradients are imposed for both solid and solute fractions.

The model is solved to steady-state, using methods implemented in R-package rootSolve (Soetaert, 2009). Mass balance is calculated in order to ensure the internal validity of the mathematical steady-state solution. At all times, the difference between the deposition flux of $aSiO_2$ and the sum of benthic fluxes of $Si(OH)_4$, burial and reprecipitation fluxes of $aSiO_2$ was < 10^{-12}.

2.2 Study site and sampling design

2.2.1 Study area

This study was conducted in the Elorn and Aulne estuaries, linking the Elorn and Aulne rivers with the Bay of Brest in northwestern France (Figure 1). The Elorn and Aulne rivers bring 85% of fresh water to the Bay of Brest - a macrotidal semi-enclosed coastal embayment subject to intense water exchanges with the Iroise Sea (semi-diurnal tidal amplitude of 4 m, 7.5 m during spring tides). The Elorn Estuary is ~ 15 km long, straight and directly exposed to marine hydrodynamics, while the Aulne Estuary is longer (~ 35 km), meandering and more protected by the Bay of Brest. The oceanic climate leads to high precipitation associated to frequent storms in winter compared to summer, thus modifying river flow. We sampled the two estuarine areas in February, April, August and November 2008 and February, May, July and October/November 2009. Except for the vertical $aSiO_2$ profiles measured in February, April and November 2008 and the proportion of highly reactive aSiO2 in sediments measured in February 2008, all the results presented here were obtained from the sampling performed in 2009.

The wind speed, the precipitation and the river flow were all higher during winter and fall than in spring and summer (Figures 2A–C). Note that a winter storm occurred just before sampling in February leading to strong winds (up to 15 kt) and high precipitation (> 25 mm d^{-1}). In winter, Elorn and Aulne River flows increased to 30 and 130 m^3 s^{-1}, respectively, during initial sampling in February, and decreased by a factor > 2 by the end of the sampling period (Figure 2C). The Aulne River flow was higher than the Elorn River flow by a factor of ~ 5 during winter, but was similar or occasionally lower than the Elorn River flow during summer. Water temperature ranged from 7.4-8.2 in winter to 16.7-19.7 in summer, and salinity varied between 0-8.7 to 20-34.2 from upper to lower estuarine stations depending on season (Table 1).

2.2.2 Surface water sampling

Surface water was sampled from salinity 0 to 35 at intervals of 5 from the center of the estuary aboard the *R/V Hésione*. Surface water was collected with a Niskin bottle, immediately stored in dark bottles in an icebox and brought back to the laboratory. Water was filtered on a polycarbonate membrane (0.6 µm pore size, 47 mm diameter) for $aSiO_2$ and $Si(OH)_4$ analyses, and on Whatman® GF/F precombusted filters (0.7 µm pore size, 47 mm diameter) for pigments analyses - e.g., chlorophyll a (Chl *a*) and phaeopigments (Phae). Polycarbonate membranes were oven-dried during 48 h and filters were stored at - 20°C until analyses. Filtered water was stored in vials at 4°C until $Si(OH)_4$ analyses.

2.2.3 Sediment and porewater sampling

Benthic sampling was performed at three stations located from upstream to downstream of Elorn (E1, E2, E3) and Aulne (A1, A2, A3) estuaries, at salinity of about ~ 0, ~ 10-20 and ~ 30 (Figure 1; Table 1). Sampling was done aboard the *R/V Hésione* at mid-tide, between the channel and the border, in subtidal sediments, based on a high spatial and temporal variability study (Raimonet et al., 2013b). A gravity corer (UWITEC®) was used to sample plexiglass cores (9.5 cm diameter × 60 cm long). Corer weight was adjusted to allow ~ 30 cm penetration into the sediment with minimal disturbance of the sediment-water interface. Geochemical measurements were done from triplicate sediment cores which were immediately sliced at 0.5 cm intervals in the first 2 cm, at 1 cm

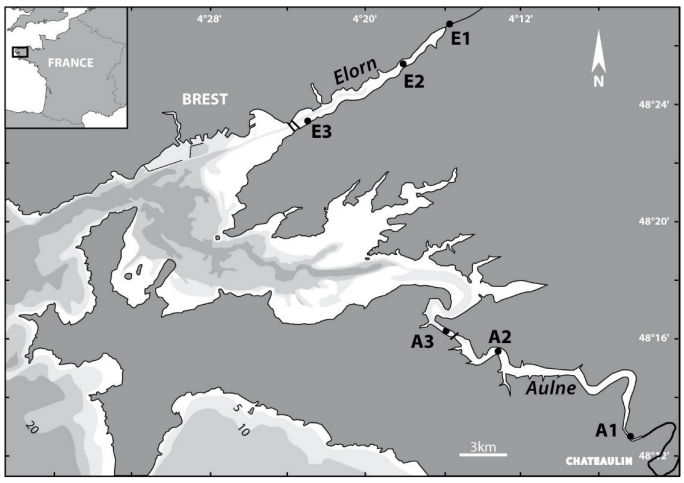

FIGURE 1
Location of benthic sampling sites along the Elorn (E1, E2, E3) and Aulne (A1, A2, A3) estuaries.

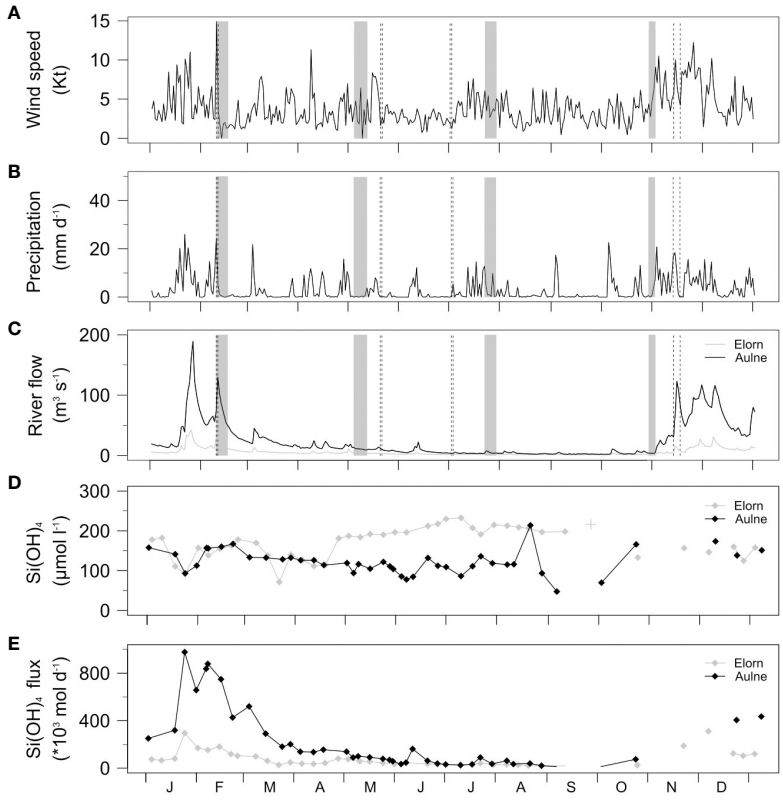

FIGURE 2
(A) Wind speed (Kt) at 10 m above the surface and **(B)** precipitations (mm d^{-1}) measured at Lanvéoc Meteo Station (Source: Meteo France). **(C)** River flow (m^3 s^{-1}) at Landerneau and 43 km upstream Chateaulin (Source: Banque Hydro). **(D)** Weekly $Si(OH)_4$ concentrations (µmol l^{-1}) at Landerneau and Chateaulin river outfalls (Source: Ecoflux). **(E)** $Si(OH)_4$ fluxes (*1000 mol d^{-1}) obtained by multiplying riverine concentrations with river flow. Pelagic and benthic sampling periods are indicated by black dashed lines and grey areas, respectively.

intervals for 2-4 cm, at 2 cm intervals for 4-12 cm, and at 4 cm intervals for 12-20 cm. Sediment sections were put in sealed 50-ml centrifugate tubes containing Vectaspin 20 filters (0.45 µm pore size, Whatman®) according to Andrieux-Loyer et al. (2008). Interstitial waters were extracted by centrifuging at 3500 rpm for 10 min (twice) at cooled temperature and acidified to pH = 2. An aliquot was preserved at 4°C for $Si(OH)_4$ analyses. Centrifuged sediments were freeze-dried for 48 h, put at 60°C to ensure complete sediment dryness and powdered for further analyses of $aSiO_2$ in the solid fraction. Subcores of 2.8 cm internal diameter were frozen with liquid nitrogen and stored at – 80°C until pigment analyses (Ni Longphuirt et al., 2006).

2.2.4 Sediment biodiffusion experiments

To measure the sediment biodiffusion rates, we used the method which consists of the vertical profile analysis of inert and fluorescent tracer introduced artificially (e.g., luminophores; Duport et al., 2006; Oleszczuk et al., 2019). Three additional sediment cores (Ø: 9.5 cm; sediment height: 30 cm; overlying water height: 40 cm) were therefore sampled at each station for these bioturbation experiments. The whole set of sediment cores was kept in controlled laboratory conditions, which mimicked the natural conditions for the estuarine temperatures and salinities (Table 1). After three days of stabilization in the controlled conditions, 3 g of luminophores (60–90 µm diameter) were homogeneously added to the overlying water and gradually spread on the sediment surface of each core without disturbing the resident infauna. Overlying water was renewed every four days with bottom water coming from each station. Cores were aerated by bubbling to keep the overlying water saturated with oxygen. Sediment cores were incubated in those conditions for 10 days, which is the minimum time to enable the characterization of the different transport modes (François et al., 1997). After this time of incubation in stable conditions, the surface water was carefully removed and cores were sliced horizontally in 0.5 cm layers from 0 to 2 cm depth, and in 1 cm layers between 2 and 10 cm depth. Each sediment layer was directly frozen to be analyzed later at the laboratory.

2.3 Field and laboratory measurements

Vertical profiles of sediment porosity: Sediment porosity in each sediment slide over depth was obtained after drying wet sediment of known volume for 5 days, after which the loss of weight was determined (Berner, 1980). This data was used to fit vertical porosity decreasing profiles.

Pelagic and benthic $aSiO_2$ contents: Pelagic $aSiO_2$ concentrations were determined using the sequential alkaline digestion method of Ragueneau et al. (2005b) and benthic $aSiO_2$ contents were

10.3389/fmars.2023.1269142

TABLE 1 Environmental parameters (temperature T, salinity S, depth D, river flow Q, tidal coefficient, $Si(OH)_4$ concentrations at the sediment-water interface C_{dSi0}) at each station and season during benthic sampling.

Station	T	S	D	Q	Tidal coefficient	C_{dSi0}
	°C	–	m	$m^3\ s^{-1}$	–	$\mu mol\ l^{-1}$
February 2009						
E1	8	0	1	18.5	108	115
E2	7.6	17.5	2	15.7	106	72
E3	8.2	29	3.5	14.5	98	25
A1	7.7	0	2.5	64.6	85	95
A2	7.4	13.7	3	54.1	70	78
A3	8	20	1.75	49.7	54	51
May 2009						
E1	12.3	0	1	4.69	51	148
E2	13.4	21.7	1.5	4.33	56	51
E3	12.8	33.5	6	4.24	64	5
A1	14.4	0	2	10.4	83	120
A2	14	22.5	3	9.95	85	44
A3	13.5	24.6	2	10.7	77	31
July 2009						
E1	16.7	0	0.5	2.79	88	100
E2	16.7	12.2	1	2.48	94	101
E3	17.7	33.5	6	1.77	102	6
A1	19.7	0	0.5	4.24	103	100
A2	19.5	27.5	1.5	5.01	105	70
A3	19.1	30.9	3	3.59	95	20
October 2009						
E1	15	0.8	0.5	1.45	38	120
E2	15.1	29.6	1.2	1.45	38	30
E3	15.3	34.2	8	1.42	49	10
A1	14.2	8.7	1	3.67	61	110
A2	15.5	29.9	1	3.47	72	28
A3	15	33	2.5	4.91	81	16

The tidal coefficient is a dimensionless number calculated from the tidal range, which characterizes the size of the tide on a scale from 20 to 120 (source: French Navy Hydrographic and Oceanographic Service).

quantified as in DeMaster (1981). Both methods allow to correct amorphous silica concentrations from lithogenic silica interference which is essential in environments rich in aluminosilicates - e.g. estuaries. Benthic $aSiO_2$ concentrations are expressed as % to refer to % g gDW^{-1}.

As $aSiO_2$ concentrations can vary from values less than 1% to more than 50% depending on study sites, we used $aSiO_2$ profiles measured in 2008 and surface $aSiO_2$ concentrations in 2009 to constrain modelled $aSiO_2$ profiles at each station. These profiles were used to estimate the range of $aSiO_2$ contents (± 1-3%) rather than to represent the fine scale vertical discontinuities (that cannot be captured by steady-state modeling). As no $aSiO_2$ profile was available for July, an annually averaged $aSiO_2$ profile of February, April and November was calculated for each station.

Vertical profiles of $Si(OH)_4$ concentrations: $Si(OH)_4$ concentrations in porewaters of each sediment slice were measured with an Auto Analyser III (Bran+Luebbe®) using the method of Tréguer and Le Corre (1975). The triplicate $Si(OH)_4$ profiles measured at each station and season in 2009 were averaged and used for fitting.

Chl a and Phae concentrations: were performed on surface water samples by using the SOMLIT protocol (http://somlit.epoc.u-

bordeaux1.fr) and on surface sediment (0.5 cm) by using a method adapted from Lorenzen (1966) and Riaux-Gobin and Klein (1993). For surface sediment, 10 ml of 90% acetone was added to each sample that was stored in the dark under constant agitation at 4°C for approximately 18 h. Chl *a* and Phae were respectively measured in the supernatant before and after acidification with a KONTRON fluorimeter (Kontron Instruments).

Proportion of highly reactive $aSiO_2$ in sediments: Dissolution experiments were carried out on 3 sediment layers (0-1, 2-3 and 6-7 cm), at all stations sampled in February 2008. The temporal increase of $Si(OH)_4$ concentrations was monitored during 21 days in batches containing the sediments and artificial seawater close to the measured *in situ* conditions: *in situ* salinity, pH of 8, constant temperature and in the dark to avoid any production of biogenic silica due to benthic organisms. The concentrations were normalized to the initial introduced Si concentrations in order to determine the dissolution rates of highly and less reactive $aSiO_2$ phases (the first and second slope of the curve). The proportion of highly reactive $aSiO_2$ was determined by statistical inverse modeling (Model 2 described in Moriceau et al., 2009). Note that we used the proportion of highly reactive $aSiO_2$ but not the dissolution rates to constrain the benthic Si model. Indeed, discrepancies between predicted and measured dissolution rates are expected in response to 1) the high detrital-to-amorphous opal ratio in our sediments (> 30%; Ragueneau and Tréguer, 1994), which increases aluminium concentrations and decreases the dissolution rate and solubility (Dixit et al., 2001); 2) the transport of fresh $aSiO_2$ to deep sediment layers by nonlocal bioturbation (Gallinari et al., 2008); 3) the absence of feedback between reprecipitation and dissolution in the model formulation (Khalil et al., 2007); 4) the cleaning of $aSiO_2$ particles from their alumino-silicate coating at the beginning of batch experiments (Khalil et al., 2007); and 5) agitation during experiments, which increases dissolution rates compared to stationary sediments (Fabre et al., 2019).

Biodiffusion coefficients: Luminophores were visualized and counted at each sediment layer by image processing (Michaud, 2006). The vertical profiles of luminophores were adjusted to a reaction diffusion type model in order to quantify biological sediment transport (Duport et al., 2006; Oleszczuk et al., 2019) and more specifically the biodiffusion-like transport coefficient (*Db*; $m^2\ d^{-1}$). The best fit between the observed and modelled tracer distribution is estimated by the least-squares method and produces the best *Db* coefficients. Sediment biodiffusion rates and depths were quantified at each station in February, July and October.

2.4 Model parameters

As detailed above, the model contains a large number of parameters that could potentially lead to multiple solutions. In order to reduce uncertainties and ensure the uniqueness of the solution calculated by the model, the strategy was to constrain parameter values with a high number of direct observations and experimental data obtained in this study, as done in (Khalil et al., 2007). All model parameters were determined from measurements and/or inverse modeling and summarized in Tables 1, 2.

Direct observations: Temperature T, salinity S and $Si(OH)_4$ concentrations in overlying water C_{dSi0} were determined from direct measurements and summarized in Table 1. Parameters ϕ_0, ϕ_∞ and $coef_\phi$ were adjusted to fit vertical porosity profile measurements (Table 2).

Assumptions based on experimental data and other measurements (Table 2): Most parameters were obtained from measurements detailed in sections 2.2 and 2.3. The biodiffusion rates D_{b0} and depths z_b were determined from ex situ experiments. Equilibrium concentrations for the two phases were assumed to be identical and equal to deep asymptotic $Si(OH)_4$ concentrations obtained from vertical profiles of $Si(OH)_4$. Based on the dissolution experiments, the proportion of highly reactive $aSiO_2$ in the deposition flux was set to 0.5 as a compromise between the low values ~ 0.3-0.5 - resulting from statistical inverse modeling of dissolution experiments performed on sediments collected in February 2008 (with the model 2 of Moriceau et al., 2009) - and the generally higher values ~ 0.5-0.9 from Khalil et al. (2007). The bioirrigation depths z_{irr} were visually adjusted to the vertically constant portions of $Si(OH)_4$ profiles where fauna was observed. Accumulation rates w were estimated from radionuclide measurements (~ 0.005 cm d^{-1}; Khalil et al., 2018). Reprecipitation rates K_p were set in the range 10^{-5}-10^{-4} d^{-1} because of the high detrital sediment content known to enhance reprecipitation rates (Khalil et al., 2007).

Inverse modeling (Table 2): was performed to estimate the values of undetermined parameters by using the package FME (Soetaert and Petzoldt, 2010). The non-linear fitting procedure using the Levenberg-Marquardt algorithm aims to minimize the sum of squared residuals of model outputs ($aSiO_2$ and $Si(OH)_4$ profiles) versus data and reproduce the curvature of these profiles. The following parameters were estimated: $aSiO_2$ deposition flux, dissolution rates of highly and less reactive $aSiO_2$ and non-local bioirrigation rate. When necessary, final adjustments were performed on the proportion of highly reactive $aSiO_2$ and reprecipitation rates. During the fitting process, upper and lower bounds in the range of expected likely values were imposed for each fitted parameter.

2.5 Benthic budgets

Model outputs (deposition fluxes of less and highly reactive $aSiO_2$, benthic fluxes of $Si(OH)_4$ including diffusion and bioirrigation, burial fluxes, reprecipitation fluxes) were used to build benthic Si budgets and to estimate the seasonal and spatial variation of fluxes at each station of the two estuaries (in mmol $m^{-2}\ d^{-1}$).

2.6 Seasonal and annual Si retention in estuaries

Fluxes of the benthic Si budgets were then extrapolated to the entire surface of each estuary and compared to river Si fluxes and pelagic production. All fluxes are presented in a conceptual scheme (Figure 3).

10.3389/fmars.2023.1269142

TABLE 2 Measured and fitted parameters used in the model for each station and season.

Parameter	Unit	Station						Source
		E1	E2	E3	A1	A2	A3	
February								
ϕ_0	–	0.76	0.84	0.84	0.85	0.86	0.87	obs
ϕ_∞	–	0.73	0.76	0.68	0.76	0.76	0.78	obs
$coef_\phi$	cm^{-1}	0.25	0.25	0.25	0.25	0.25	0.25	obs
D_{b0}	$cm^2\ h^{-1}$	5.71E-05	9.70E-05	6.85E-05	2.85E-06	2.28E-06	3.20E-05	obs
$coef_b$	cm^{-1}	1	1	1	1	1	1	obs
z_b	cm	7.5	7.5	5	0	1.5	2	obs
C_{dSieqF}	$\mu mol\ l^{-1}$	260	325	330	505	400	400	obs
C_{dSieqS}	$\mu mol\ l^{-1}$	260	325	330	505	400	440	obs
w	$cm\ h^{-1}$	2.00E-04	2.00E-04	2.00E-04	2.00E-04	2.00E-04	2.00E-04	obs
p_{aSiF}		0.5	0.5	0.5	0.5	0.5	0.5	obs/fitted
z_{irr}	cm	8	12	15	0	0	10	obs/fitted
α		3.60E-02	1.80E-03	8.64E-04	0.00E+00	0.00E+00	1.15E-03	obs/fitted
K_{aSiF}	h^{-1}	3.46E-05	4.00E-05	2.00E-05	2.08E-04	4.00E-04	2.50E-05	fitted
K_{aSiS}	h^{-1}	3.46E-08	8.33E-06	5.00E-06	1.04E-06	4.17E-07	2.08E-06	fitted
K_p	$\mu mol\ l^{-1}$	1.00E-04	1.00E-07	1.00E-04	1.00E-06	1.00E-03	0.000001	fitted
C_{dSieqP}	$\mu mol\ l^{-1}$	100	200	200	200	200	200	fitted
May								
ϕ_0	–	0.89	0.87	0.85	0.92	0.86	0.91	obs
ϕ_∞	–	0.81	0.74	0.72	0.81	0.62	0.79	obs
$coef_\phi$	cm^{-1}	0.81	0.25	0.27	0.13	0.12	0.86	obs
D_{b0}	$cm^2\ h^{-1}$	9.13E-05	1.35E-04	1.06E-04	5.71E-07	2.28E-06	3.20E-05	obs
$coef_b$	cm^{-1}	1	1	1	1	1	1	obs
z_b	cm	11.25	11.25	7	0.25	2.5	3.25	obs
C_{dSieqF}	$\mu mol\ l^{-1}$	200	300	300	425	365	470	obs
C_{dSieqS}	$\mu mol\ l^{-1}$	200	380	300	425	365	470	obs
w	$cm\ h^{-1}$	2.00E-04	2.00E-04	2.00E-04	2.00E-04	2.00E-04	2.00E-04	obs
p_{aSiF}		0.5	0.5	0.5	0.5	0.5	0.5	obs/fitted
z_{irr}	cm	11	8	11	0	0	7	obs/fitted
α		3.60E-02	7.20E-03	3.60E-02	0.00E+00	0.00E+00	4.32E-02	obs/fitted
K_{aSiF}	h^{-1}	4.17E-04	3.00E-05	5.00E-05	5.00E-05	2.00E-05	3.00E-05	fitted
K_{aSiS}	h^{-1}	4.17E-06	5.00E-07	1.39E-06	5.00E-07	4.17E-07	2.00E-06	fitted
K_p	$\mu mol\ l^{-1}$	1.00E-04	1.00E-05	1.00E-07	1.00E-06	1.00E-03	1.00E-06	fitted
C_{dSieqP}	$\mu mol\ l^{-1}$	200	200	200	200	200	200	fitted
July								
ϕ_0	–	0.88	0.88	0.81	0.93	0.75	0.81	obs
ϕ_∞	–	0.77	0.77	0.72	0.85	0.72	0.75	obs
$coef_\phi$	cm^{-1}	0.16	0.54	0.56	0.25	0.25	0.25	obs

(Continued)

10.3389/fmars.2023.1269142

TABLE 2 Continued

Parameter	Unit	Station						Source
		E1	E2	E3	A1	A2	A3	
D_{b0}	$cm^2\ h^{-1}$	1.26E-04	1.71E-04	1.43E-04	5.71E-07	1.71E-06	1.71E-06	obs
$coef_b$	cm^{-1}	2	2	2	2	2	2	obs
z_b	cm	15	15	9	0.5	3.5	3.5	obs
C_{dSieqF}	$\mu mol\ l^{-1}$	290	275	400	325	260	520	obs
C_{dSieqS}	$\mu mol\ l^{-1}$	290	275	400	325	260	520	obs
w	$cm\ h^{-1}$	2.00E-04	2.00E-04	2.00E-04	2.00E-04	2.00E-04	2.00E-04	obs
p_{aSiF}		0.5	0.5	0.5	0.5	0.5	0.5	obs/fitted
z_{irr}	cm	13	11	8	0	4	7	obs/fitted
α		7.20E-03	1.08E-02	7.20E-03	0.00E+00	6.48E-03	6.12E-03	obs/fitted
K_{aSiF}	h^{-1}	1.00E-04	3.00E-05	6.00E-05	4.00E-05	2.00E-05	4.00E-05	fitted
K_{aSiS}	h^{-1}	2.08E-07	4.17E-06	1.04E-06	1.00E-06	2.08E-06	2.00E-08	fitted
K_p	$\mu mol\ l^{-1}$	5.00E-04	1.00E-06	1.00E-07	1.00E-07	1.00E-05	1.00E-07	fitted
C_{dSieqp}	$\mu mol\ l^{-1}$	200	200	200	200	200	200	fitted
October								
ϕ_0	–	0.90	0.87	0.77	0.90	0.80	0.94	obs
ϕ_∞	–	0.72	0.72	0.72	0.83	0.72	0.79	obs
$coef_\phi$	cm^{-1}	0.18	0.28	0.25	0.10	0.10	1.17	obs
D_{b0}	$cm^2\ h^{-1}$	9.13E-05	1.35E-04	1.06E-04	5.71E-07	2.28E-06	3.20E-05	obs
$coef_b$	cm^{-1}	2	2	2	2	2	2	obs
z_b	cm	11.25	11.25	7	0.25	2.5	3.25	obs
C_{dSieqF}	$\mu mol\ l^{-1}$	320	300	425	250	285	420	obs
C_{dSieqS}	$\mu mol\ l^{-1}$	320	300	425	250	285	420	obs
w	$cm\ h^{-1}$	2.00E-04	2.00E-04	2.00E-04	2.00E-04	2.00E-04	2.00E-04	obs
p_{aSiF}		0.5	0.5	0.5	0.5	0.5	0.5	obs/fitted
z_{irr}	cm	19	12	6	0	5	8	obs/fitted
α		6.12E-03	6.12E-03	8.00E-03	0.00E+00	9.00E-03	1.80E-03	obs/fitted
K_{aSiF}	h^{-1}	2.00E-05	3.00E-05	2.00E-05	2.00E-05	1.07E-05	2.00E-05	fitted
K_{aSiS}	h^{-1}	2.08E-07	4.17E-06	1.00E-06	8.33E-07	2.08E-07	1.00E-06	fitted
K_p	$\mu mol\ l^{-1}$	2.00E-04	1.00E-05	1.00E-05	1.00E-05	1.00E-05	1.00E-07	fitted
C_{dSieqp}	$\mu mol\ l^{-1}$	200	200	200	200	200	200	fitted

River Si fluxes were determined as the sum of $Si(OH)_4$ and $aSiO_2$ fluxes. $Si(OH)_4$ fluxes were estimated as the product of weekly $Si(OH)_4$ concentrations (from the citizen-science network ECOFLUX; Abbott et al., 2018) by weekly river flow (from Banque Hydro) at the outlet of Elorn and Aulne rivers. $aSiO_2$ fluxes were estimated as the product of seasonal $aSiO_2$ concentrations (this study) by the same weekly river flow. Weekly fluxes were summed to obtain seasonal and annual fluxes.

Deposition, burial and benthic $Si(OH)_4$ fluxes were estimated by multiplying modelled fluxes at the 3 stations of the 2 estuaries (section 2.5) by the estuary surface of each estuarine section in order to estimate the retention of Si in the estuaries (in kmol) at the seasonal and annual scales. The surface of spatial integration for the 3 stations in each estuary was determined using a GIS-based approach (Khalil et al., 2018).

Burial fluxes in tidal saltmarshes were estimated for saltmarshes invaded and non-invaded by *Spartina alterniflora* in the Elorn estuary (Querné, 2011). The ratio of intertidal burial over subtidal burial was calculated for the Elorn estuary (0.69) and used to estimate intertidal burial in the Aulne estuary.

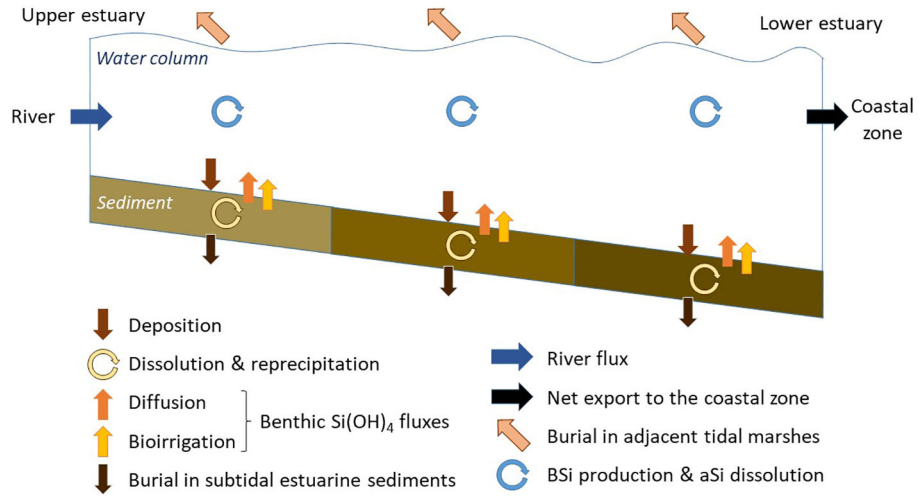

FIGURE 3
Conceptual scheme presenting fluxes of the Si budget along the estuary. The size of arrows is not proportional to quantified fluxes.

Export was the difference between river fluxes and burial (in subtidal sediments and in intertidal saltmarches).

Pelagic primary production was estimated as the sum of pelagic production rates (measured in this study at salinity 0, 5, 10, 15, 20, 25 and 30) vertically integrated on the seven estuarine boxes in each estuary for each season. Incubations were performed at *in situ* conditions (temperature, attenuated light) for 24h with ^{14}C tracer following the method of Le Bouteiller et al. (2003). The range of pelagic BSi production rates was estimated by multiplying carbon primary production rates by the Si:C factor of 0.03 and 0.13. The factor 0.13 is characteristic of 100% diatoms and preservation, while 0.03 is used to consider that only 25% is related to diatoms and/or preserved. The volume of spatial integration was described with a power function (Eq. 9; Soetaert et al., 2006) and validated with morphological observations (Bassoulet, 1979; Google Map©; this study).

$$x = x_{riv} + (x_{riv} - x_{sea})\frac{x^a}{x^a + (ks_a)^a} \quad (9)$$

with x is the estuary volume. x_{riv} and x_{sea} are the values at the freshwater and marine water end-members of the estuary, respectively. The exponent *a* regulates the steepness of the relationship.

3 Results

3.1 $Si(OH)_4$, $aSiO_2$ and Chl *a* in estuarine waters

Temporal changes of $Si(OH)_4$ loads at the freshwater end-member

The $Si(OH)_4$ concentrations at the freshwater end-member (station E1 and A1) were similar in Elorn and Aulne from December to April (140 ± 29 and 140 ± 22 µmol l^{-1}, respectively), but were higher in Elorn from May to September (203 ± 15 and 108 ± 31 µmol l^{-1}, respectively; Figure 2D).

The $Si(OH)_4$ fluxes at the freshwater end-member were higher 1) in winter when the river flow increased, and 2) in the Aulne River from December to April (42 ± 30 t d^{-1} for the Aulne River, versus 7 ± 5 t d^{-1} for the Elorn River; Figure 2E). The fluxes were lower and more similar from May to October (5 ± 4 t d^{-1} in the Aulne River versus 2 ± 1 t d^{-1} in the Elorn River), but they were occasionally higher at the mouth of the Elorn River in July and October (Figure 2E). The relative contribution of the Aulne River to the $Si(OH)_4$ fluxes in the Bay of Brest ranged from a minimum of 40% in summer to a maximum of 80% in winter.

Seasonal distributions of $Si(OH)_4$, $aSiO_2$, and Chl a concentrations along the estuaries

The $Si(OH)_4$ concentrations behaved almost conservatively and continuously decreased along the salinity gradients of both the Elorn and Aulne estuaries at all seasons except July (Figure 4A). In the Elorn Estuary, the $Si(OH)_4$ concentrations were similar at these three seasons. In the Aulne Estuary, the $Si(OH)_4$ concentrations at the freshwater end-member decreased from fall/winter to spring/summer, leading to seasonal variations of the slope. In summer, the curve was no longer conservative, which suggested $Si(OH)_4$ consumption in both estuaries. Note that the $Si(OH)_4$ (and $aSiO_2$; Figure 4B) concentrations at the freshwater end-member in the Elorn Estuary were lower than at salinity 5 in February. This non conservative profile resulted probably from the transient increase of river flow (Figure 2C) as explained by Regnier et al. (1998).

In both estuaries, the $aSiO_2$ concentrations decreased with increasing salinity at all seasons, except July (Figure 4B). In the Aulne Estuary, a steep decrease of $aSiO_2$ concentrations occurred between salinity 0 and 5. The highest $aSiO_2$ concentrations were observed in July and reached a maximum at the salinity range of 5-15 (data not available for the Elorn Estuary).

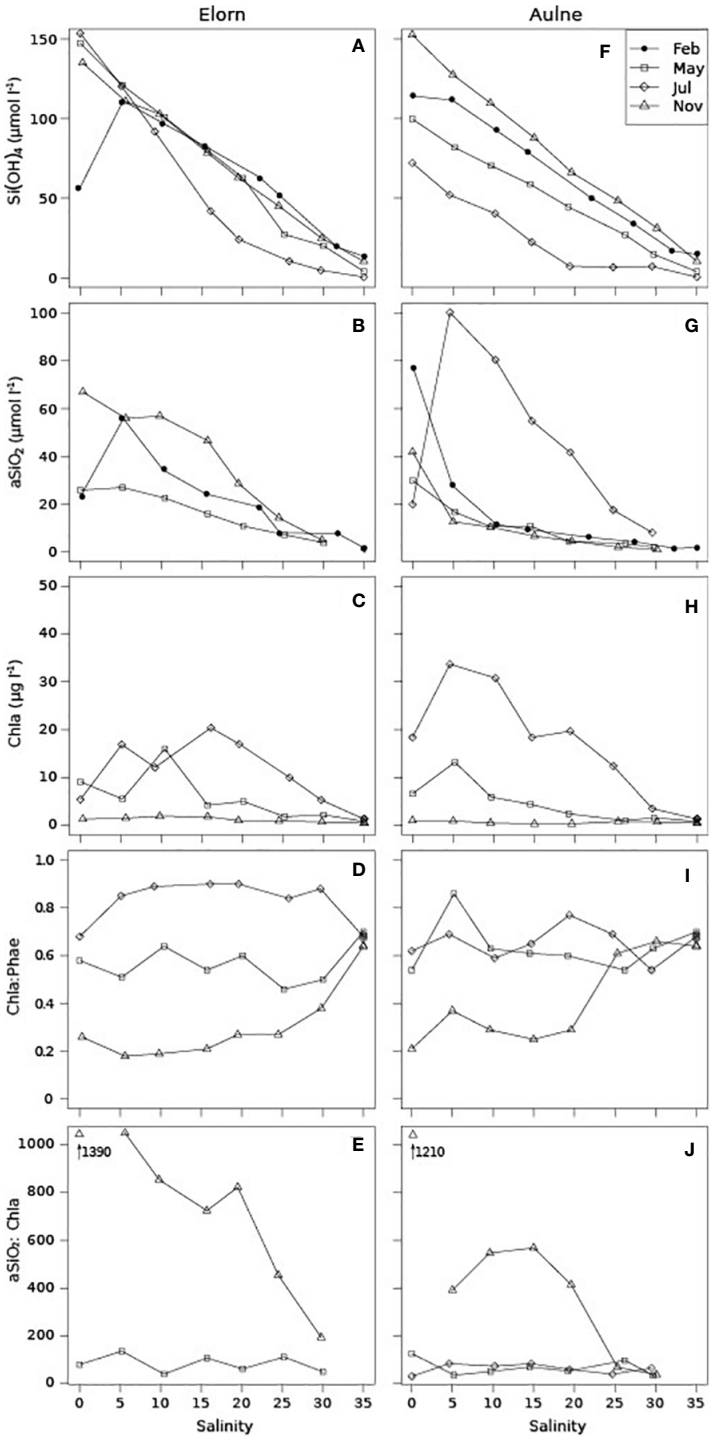

FIGURE 4
Pelagic $Si(OH)_4$, $aSiO_2$ and Chl *a* concentrations, Chl *a*: (Chl *a*+Phea) ratios, and $aSiO_2$: Chl *a* ratios, along the Elorn Estuary **(A–E)** and the Aulne Estuary **(F–J)**, in February, May, July and November 2009.

In spring and summer, maximal concentrations of Chl *a* were generally observed between salinity 5 and 20, as observed for $aSiO_2$ concentrations in July. In November, Chl *a* concentrations were low and constant with salinity, which completely differed from the high and decreasing $aSiO_2$ concentrations. In both estuaries, the Chl *a*: (Chl *a*+Phae) ratios were higher in spring/summer than in winter and reached an annually constant marine end-member ratio in the range 0.6-0.7 (Figure 4D). The $aSiO_2$:Chl *a* ratios were low in spring/summer and very high in winter, especially in upper estuaries (Figure 4E).

3.2 Surface sediments $aSiO_2$ and Chl *a* along estuaries

The $aSiO_2$ concentrations were in the range 0.5-3% in the surface sediments (Figure 5A). At each season, they decreased from upstream to downstream in the Elorn Estuary, and they were minimal at the intermediate station in the Aulne Estuary (Figure 5A). At all stations, surface Chl *a* concentrations increased from February to July, and then decreased in November (Figure 5B). The Chl *a*:(Chl *a*+Phae) ratios were always > 0.4 (Figure 5C). The $aSiO_2$:Chl *a* ratios decreased from February to July regardless of station, and from upstream to downstream in winter (Figure 5D).

3.3 Benthic Si cycle along estuaries: data and modeling

Observed and simulated $aSiO_2$ and $Si(OH)_4$ profiles

The observed $aSiO_2$ profiles were vertically constant with small discontinuities along the sediment cores. The model represented well the range of $aSiO_2$ concentrations but failed to reproduce the small vertical heterogeneities. Although variable between stations, $Si(OH)_4$ concentrations in general increased with depth (Figure 6; black circles). A regular hyperbolic profile, commonly observed in stable or oceanic sediments, was observed at station A1, while stations E1, E2, E3, and A3 showed concentrations that became stable over the first centimeters (of variable thickness) which then increased again at greater depths. In general the model provided a good fit to the observed $Si(OH)_4$ trends, with the exception of the subsurface maxima of $Si(OH)_4$ concentrations observed at station A2 in February and May (Figure 6).

Estimated and calibrated parameters

The biodiffusion rates of sediments (obtained from core incubations with luminophores) increased from February to July (Table 2). These rates were higher in the Elorn (1-4 10^{-7} m^2 d^{-1}) than in the Aulne Estuary (< 1 10^{-7} m^2 d^{-1}), and they were almost null at stations A1 and A2. The bioirrigation rates varied relatively similarly to biodiffusion rates (Table 2). The calibrated dissolution rates of the less reactive $aSiO_2$ were in the range 10^{-5}- 2 10^{-4} d^{-1} (Table 2). The lowest rates were observed at stations E1 and A2. The calibrated dissolution rates of the highly reactive $aSiO_2$ were in the range 10^{-3}- 2 10^{-2} d^{-1} (Table 2), and generally increased from February to July or October; however, at stations A1 and A2, the highest rates were found in February. Reprecipitation rates generally varied between 10^{-5} and 10^{-4} d^{-1}.

Simulated fluxes

The simulated deposition fluxes of $aSiO_2$ were in the range 2-4.5 mmol m^{-2} d^{-1}, regardless of season and station (Figure 7A). In both estuaries, maximal deposition fluxes were observed upstream of the estuaries in winter, and midstream/downstream during other seasons. The burial fluxes of the less and highly reactive $aSiO_2$ were 25-80% of the deposition flux of $aSiO_2$ (Figures 7B, C, 8). In the Elorn Estuary and at station A3, the proportion of burial decreased from winter to summer. This decrease was due to an increase of sediment-water $Si(OH)_4$ effluxes by diffusion and non-

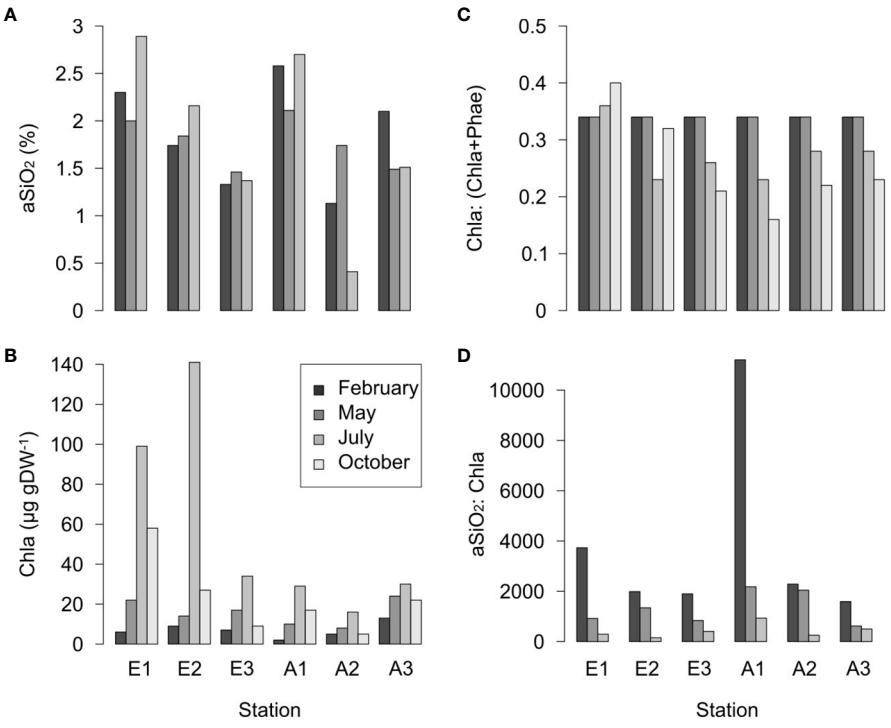

FIGURE 5
(A) $aSiO_2$ content (%), **(B)** Chl *a* concentrations (µg l^{-1}), **(C)** Chl *a*: (Chl *a*+Phea) and **(D)** $aSiO_2$: Chl *a* ratios measured at each season (February, May, July, October 2009) in superficial sediments at the stations 1, 2 and 3 (n = 3) of the Elorn and Aulne estuaries.

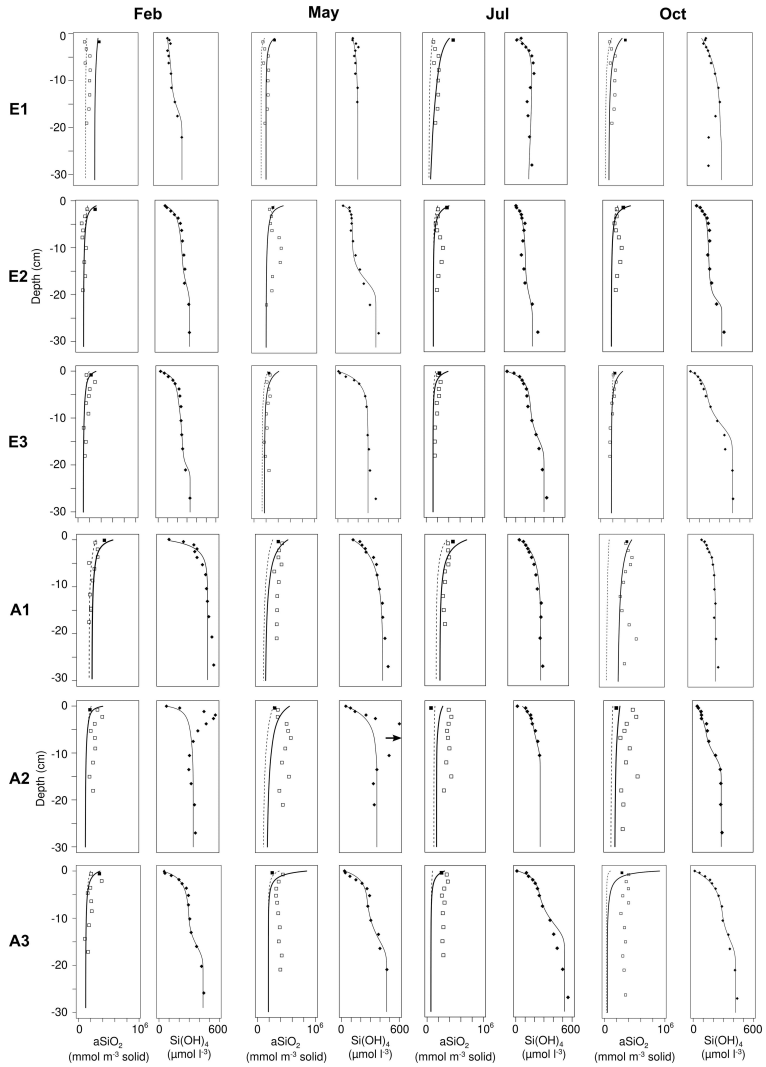

FIGURE 6
$Si(OH)_4$ and $aSiO_2$ concentrations in benthic sediments at each station (1, 2, 3) of Elorn and Aulne estuaries in February, May, July and October 2009. Both data from 2008 (cross) and 2009 (points) and model outputs (lines) are represented. For $aSiO_2$, the continuous line represents the total concentration while the dashed line represents the less reactive fraction.

local bioirrigation, with a generally higher contribution of bioirrigation (Figures 7E, F). The decrease of burial fluxes in summer is not observed at stations A1 and A2, where bioirrigation is low. Reprecipitation fluxes were generally < 5% regardless of station and season (Figures 7D, 8).

3.4 Seasonal and annual Si retention in Elorn and Aulne estuaries

The Aulne river-estuary had a larger contribution than the Elorn river-estuary to all fluxes because of the larger size of its watershed and estuary. The Table 3 summarizes the estuarine Si budget and retention for the Elorn, Aulne and the two estuaries, at seasonal and annual scales.

As previously observed (Figure 2E), total Si river fluxes are two to three orders of magnitude higher in winter (134074 kmol per season) than in summer (8417 kmol per season). The Si loads are dominated by $Si(OH)_4$ in both estuaries (64 to 90% from winter to summer). Compared to the Elorn river, the Aulne river brings 66 to 90% of river Si fluxes to the Bay of Brest from summer to winter.

Deposition fluxes are similar for all seasons (8570-10784 kmol per season) but strongly vary from 6% of river loads in winter to more than 100% during summer.

Recycling leads to benthic fluxes of $Si(OH)_4$ ranging from 3585 kmol in winter to 6409 kmol in summer. Bioirrigation accounts for 46% of benthic fluxes (15-68%), with stronger bioirrigation in the Elorn estuary (64-68%) than in the Aulne estuary (15-34%). During summer, benthic recycling (6409 kmol) provides a quantity of $Si(OH)_4$ close to river fluxes (7348 kmol $Si(OH)_4$; 87% of 8417 kmol total Si).

The reprecipitation flux is low and negligible with 168 kmol per year for the two rivers.

Burial in subtidal sediments accounts for 10-39% of river Si loads in the Elorn estuary and 3-38% in the Aulne estuary, from

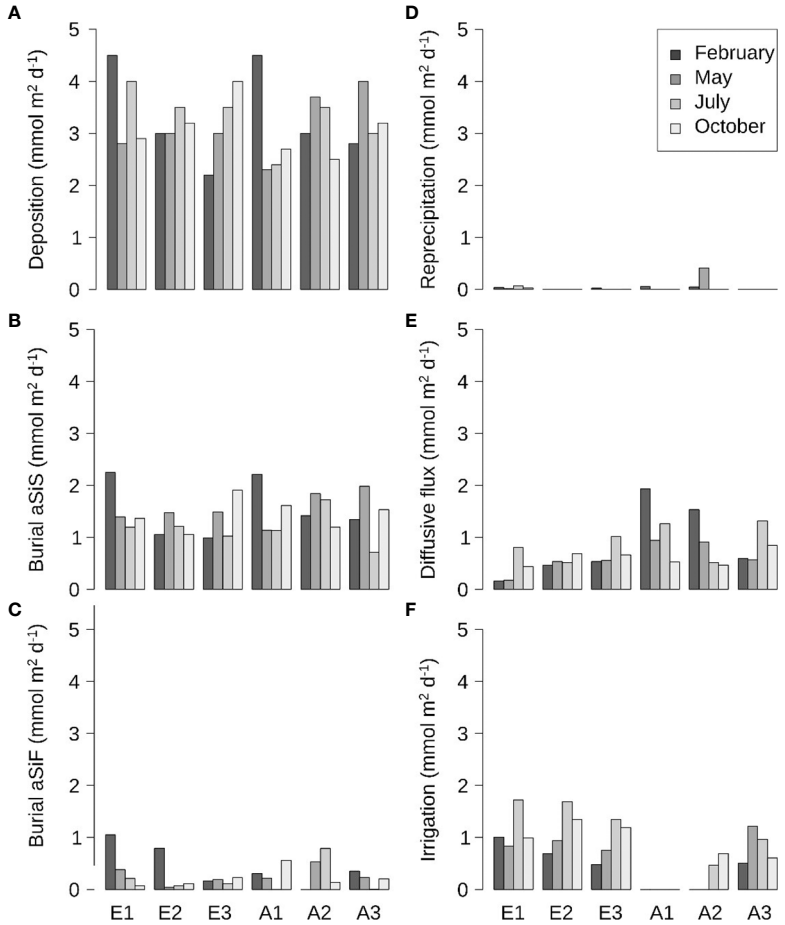

FIGURE 7
Benthic Si budget: **(A)** deposition flux of $aSiO_2$, **(B)** burial flux of less reactive $aSiO_2$, **(C)** burial flux of highly reactive $aSiO_2$, **(D)** reprecipitation flux, **(E)** benthic diffusive flux of $Si(OH)_4$, and **(F)** non-local bioirrigation flux, for stations E1, E2, E3, A1, A2 and A3 at all seasons.

winter to summer. Burial in tidal marshes is estimated to ~2/3 of subtidal burial (based on data on the Elorn estuary; Querné, 2011). Including burial in tidal marshes leads to an estimated burial of 17-41% of river Si loads in the Elorn estuary and 16-64% in the Aulne estuary.

Finally, export is high during winter and fall (125 649 kmol; 93% of river flux; 51% of annual export flux), but lower during summer (2 779 kmol; 33% of river flux; 1% of annual export flux).

4 Discussion

4.1 Seasonality of $aSiO_2$ deposition and quality along Elorn and Aulne estuaries

In this study, steady-state diagenetic modeling is used to quantify the averaged benthic processes at seasonal scale along two estuaries. Modeling is particularly efficient for determining the deposition fluxes, which otherwise are very difficult to assess by direct measurements (Ridd et al., 2001). Regardless of the station and season, the deposition fluxes in the Elorn and Aulne estuaries (2-4.5 mmol m^{-2} d^{-1}; Figure 7A) are in the same order of magnitude than in the seaward Bay of Brest (0.6-3 mmol m^{-2} d^{-1}; Ragueneau et al., 2005a). These high deposition fluxes are consistent with the high accumulation rates measured through radionuclide measurements that constrain the model (Khalil et al., 2018). High deposition and accumulation of $aSiO_2$ are generally observed seaward in large rivers (e.g., the Amazon, Congo, and Yangtze rivers; DeMaster et al., 1985; Shiller, 1996; Raimonet et al., 2015) that have high river flow rates. In contrast, in our study, the $aSiO_2$ deposition fluxes are high in the estuary due to lower river flow rate and the semi-enclosed shape of the system. These deposition fluxes calculated in the macrotidal Aulne and Elorn estuaries are in the range of values determined for the macrotidal Scheldt river and estuary: from ~0.028-0.034 mmol m^{-2} d^{-1} in subtidal sediments in the Scheldt river (Carbonnel et al., 2009), to ~1.6 mmol m^{-2} d^{-1} in marsh sediments in the Scheldt estuary (Struyf et al., 2006) and a maximum of 8 mmol m^{-2} d^{-1} in subtidal sediments in the Scheldt river/estuary (Arndt and Regnier, 2007).

In this study, maximal deposition fluxes are observed upstream of the estuaries during winter, which is mostly related to higher $aSiO_2$ river concentrations and fluxes. High $aSiO_2$ concentrations and fluxes brought to the estuary are related to enhanced soil weathering and river flows (Figure 2C), as previously reported by

10.3389/fmars.2023.1269142

TABLE 3 River Si fluxes compared to deposition, benthic fluxes including bioirrigation, reprecipitation, subtidal and tidal marsh burial, and export (kmol per year and per season) for the Elorn and Aulne estuaries.

	Total Elorn+Aulne					Elorn					Aulne				
	Annual	Winter	Spring	Summer	Autumn	Annual	Winter	Spring	Summer	Autumn	Annual	Winter	Spring	Summer	Autumn
River flux	277321	134074	24262	8417	110568	35239	13349	5163	2855	13872	242081	120724	19099	5562	96696
including $Si(OH)_4$ flux	80%	75%	83%	87%	75%	83%	85%	86%	90%	69%	77%	64%	80%	85%	81%
Deposition	38944	8570	10784	9622	9967	11973	2311	2808	3303	3551	26971	6259	7976	6319	6416
Benthic fluxes	19135	3585	4586	6409	4555	6207	990	1259	2194	1764	12929	2595	3328	4215	2791
including bioirrigation	46%	40%	45%	49%	50%	66%	64%	68%	67%	66%	25%	15%	23%	30%	34%
Reprecipitation	168	40	120	3	5	24	16	1	2	4	144	24	119	1	1
Subtidal burial	19639	4944	6078	3210	5407	5742	1304	1548	1107	1783	13897	3639	4530	2104	3625
Tidal marsh burial	*13473*	*3481*	*4092*	*2428*	*3471*	3939	*985*	*985*	*985*	*985*	*9534*	*2496*	*3108*	*1443*	*2486*
Export	*244209*	*125649*	*14092*	*2779*	*101689*	*25558*	*11060*	*2630*	*764*	*11105*	*218650*	*114588*	*11462*	*2015*	*90585*

Smis et al. (2011). These winter deposition fluxes are associated with detrital $aSiO_2$, as shown by high $aSiO_2$:Chl *a* and low Chl *a*:(Chl *a* +Phae) benthic ratios (Figure 5).

Deposition is observed more downstream and all along the estuary in spring and summer. The matter deposited then is also more reactive because of a higher contribution of riverine and estuarine, pelagic and benthic, primary production, stimulated by increasing light and temperature, often observed in estuaries (Heip et al., 1995).

The increase in river primary production (either benthic and/or pelagic) is highlighted by a decrease in $Si(OH)_4$ concentrations (consumption) and an increase in Chl *a* concentrations at the freshwater end-members from winter to summer (Figures 2, 4). This riverine material generally settles before salinity 5 (Anderson, 1986) and fuels deposition in the upper estuary.

The contribution of estuarine pelagic primary production to $aSiO_2$ deposition in the two estuaries is highlighted by an increase in Chl *a* and $aSiO_2$ concentrations in the water column at salinity 5-20, and decreasing $aSiO_2$: Chl *a* ratios (Figures 4, 5), as well as production estimates along estuaries (estimated to be 57-225 10^3 mol d^{-1} from incubations performed in this study). Benthic primary production (subtidal or intertidal by lateral transport) are suggested by the Chl *a* concentrations in surface sediments at stations E1 and E2 that are 4-15 times higher than in Aulne Estuary in summer, whereas Chl *a* concentrations in the water column are similar in both estuaries. This pelagic and benthic production must have settled inside the estuary depending on tidal range and river flow.

The relatively low increase of deposition fluxes during summer compared to winter (Figure 7A), as well as lower benthic than pelagic Chl *a*:(Chl *a*+Phae) ratios in summer (Figures 4D, 5C), also suggest the enhancement of pelagic dissolution in summer; dissolution increases the degradation state of deposited $aSiO_2$ and decreases the quantity of $aSiO_2$ at the sediment-water interface. Pelagic dissolution has been estimated to account for ~ 50% of pelagic $aSiO_2$ production in the Bay of Brest (Beucher et al., 2004) and > 80% in estuaries reaching the Chesapeake Bay (Anderson, 1986), and is expected to be enhanced by bacterial degradation in estuaries (Roubeix et al., 2008a). Moreover, the constant benthic Chl *a*:(Chl *a*+Phae) ratios observed from winter to spring, which decrease during the summer and co-occur with the highest pelagic ratios, suggests enhanced benthic macrofauna grazing (Cariou-Le Gall and Blanchard, 1995), alterations caused by light (Nelson, 1993) and redox conditions (Sun et al., 1993). All of these results confirm the estimation of 50% highly reactive $aSiO_2$ calculated through an inverse statistical method (Moriceau et al., 2009) and used in our diagenetic model of benthic Si cycle.

4.2 Seasonal benthic Si budgets along estuaries

As suggested in the previous section, deposition fluxes are tightly related to seasonal changes of river fluxes, detrital loads, benthic and pelagic primary production, and/or lateral transport. Once $aSiO_2$ is deposited at the sediment-water interface, benthic

processes lead either to the return of Si to the water column through dissolution and/or bioirrigation, or to its sequestration in sediments through burial and/or reprecipitation.

The formation of $Si(OH)_4$ through benthic recycling is known to potentially suffer reverse weathering in benthic sediments (Michalopoulos and Aller, 2004). Indeed, very high reprecipitation has even been reported in high-detrital sediments of the subtropical Amazon delta, in which ~ 90% of initial benthic $aSiO_2$ has been converted to clay (Michalopoulos and Aller, 2004), or in the Mississippi River Delta, where it accounts for ~ 40% of Si storage (Presti and Michalopoulos, 2008) or in the Barentz Sea (37% at station B13; Ward et al., 2022). In our study, the reprecipitation processes are limited, and reprecipitation fluxes estimated by the model are < 5% of deposition fluxes regardless of station (Figure 8). This is consistent with the values found in the Scheldt Estuary (Rebreanu, 2009). Laboratory experiments are however needed to confirm our model estimates.

The high burial fluxes determined in this study may be linked to 1) high deposition fluxes related to high $aSiO_2$ fluxes coming from rivers (high concentrations during high river flow; Figures 2C, 4B), 2) high detrital and aluminium contents, which increase $aSiO_2$ preservation (Van Cappellen et al., 2002), 3) the macrotidal regime and associated resuspension events, which increase recycling in the water column (Gehlen and Van Raaphorst, 2002), which decreases $aSiO_2$ reactivity, and 4) bioturbation and more specifically sediment mixing, which increases the transfer of newly settled $aSiO_2$ deeper in the sediment and increases its preservation, as observed in organic matter (Aller and Mackin, 1984). Such high burial rates have already been observed in highly accumulating zones, e.g., Antarctic sediments in which one third of $aSiO_2$ deposited accumulates in sediments (Pondaven et al., 2000; DeMaster, 2002). On the contrary, estuaries of large rivers (e.g., Amazon, Congo) have low retention due to export to the coastal margins where deposition and accumulation take place (Michalopoulos and Aller, 2004; Dürr et al., 2011; Raimonet et al., 2015).

In summer, the estimated fluxes are similar to those observed within the Bay of Brest during the productive period, where burial fluxes were estimated to be ~ 32% (Ragueneau et al., 2005a). However, distinct processes cause these similar proportions. In the Bay of Brest, the absence of total recycling is explained by the presence of an invasive filter feeder species, *Crepidula fornicata*, that increases $aSiO_2$ preservation in sediments through 1) its incorporation in feces covered by organic matter, and 2) the presence of aluminium-rich sediments (Ragueneau et al., 2005a). In the Elorn and Aulne estuaries, invasive species are absent at the sediment-water interface, and the high burial fluxes are instead explained by the enhanced preservation due to high aluminium and detrital contents (Van Cappellen et al., 2002), high deposition rates (Aller and Mackin, 1984; Conley and Johnstone, 1995), and burrowing depth reaching more than 20 cm in depth.

During the productive period, particularly during summer, the increased proportion of $Si(OH)_4$ fluxes associated to dissolution and bioirrigation (> 60%; Figure 8) compared to burial fluxes is explained by the enhancement of dissolution rates by temperature (Kamatani, 1982; Ragueneau et al., 2002a) as well as deposition of more reactive (autochthonous) material, and bioirrigation (Green et al., 2004).

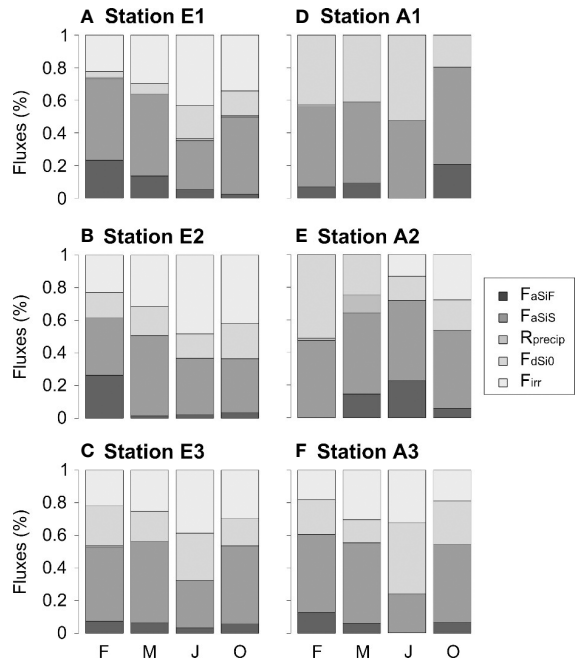

FIGURE 8
Benthic Si budget: proportion of each flux in February, May, July and October (noted F, M, J and O, respectively), for **(A)** station E1, **(B)** station E2, **(C)** station E3, **(D)** station A1, **(E)** station A2 and **(F)** station A3.

4.3 Seasonal contribution of benthic silica cycle to the estuarine filter

First, our study confirms the importance to include $aSiO_2$ when investigating Si retention in estuaries (Carbonnel et al., 2013) or building global silica budgets (Tréguer et al., 2021).

Regardless of the method used, estuarine budgets do not generally explicitly account for the benthic ecosystem in estuaries, due to the assumed small contribution of benthic fluxes compared to that of river fluxes (Arndt et al., 2009). However, benthic sediments may be subject to non-local transport associated with bioirrigation, which is known to strongly increase benthic $Si(OH)_4$ fluxes at the sediment-water interface (Marinelli, 1992; Forja and Gómez-Parra, 1998), and this is also observed in our study (~50%). Although Arndt and Regnier (2007) have recently analytically resolved benthic processes in a reactive-transport silica model which couples benthic and pelagic processes, methods used to estimate estuarine Si budgets do not vertically resolve the nonlocal benthic processes, e.g., bioirrigation. Contrary to reactive-transport modeling of water column processes, which provides high spatio-temporal resolution, the goal of the present study is to precisely investigate benthic processes in Elorn and Aulne estuary sediments in order to build Si budgets. Our results show the usefulness to incorporate irrigation effects in reactive-transport modeling along estuaries.

During winter floods, the high river flows increase the $aSiO_2$ and $Si(OH)_4$ river fluxes to both estuaries as well as the export to the coastal waters (Table 3). This transient and high export of particulate matter, mostly detritic (see section 4.1), has previously been observed in this ecosystem for organic matter (Savoye, 2001). The increase in river flow also decreases the contribution of benthic $Si(OH)_4$ fluxes (2.7%), $aSiO_2$ burial (3.7%) and $aSiO_2$ deposition fluxes (6.4%) compared to $aSiO_2$ river fluxes. These results confirm that generally low benthic-pelagic coupling occurs during high river flow conditions (Eyre and Ferguson, 2006).

From winter to summer, the drop in the river flow reduces $aSiO_2$ and $Si(OH)_4$ fluxes and increases water residence times throughout the estuary. The $aSiO_2$ deposition becomes higher than river fluxes (Table 3), which highlights that other sources become significant in fueling the sediment-water interface: not only river loads, but also pelagic primary production in the estuary, lateral transport from intertidal sediments or from mixing of marine waters.

First, the $aSiO_2$ deposition fluxes are enhanced by the increase in pelagic primary production in summer. This is highlighted by the high Chl *a* concentrations measured in May and even more in July (from 6 to 35 $\mu g\ l^{-1}$ along the salinity gradient; Figure 4C). Note that these concentrations are higher than those in the Bay of Brest (generally < 10 $\mu g\ l^{-1}$ even during blooms, except a maximum of 21 $\mu g\ l^{-1}$ observed in 1981; Chauvaud et al., 2000), and that even higher concentrations have already been measured in these estuaries during summer (88 and 46 $\mu g\ l^{-1}$; Savoye, 2001). In this study, the extrapolation of the pelagic primary production measurements in the Aulne Estuary allows us to roughly estimate a total pelagic primary production of ~ 57-225 10^3 mol d^{-1}. This estimate is slightly lower than the production of 448 10^3 mol d^{-1} estimated in the Bay of Brest (Ragueneau et al., 2002a). However, this estimation is close to the deposition flux (107 10^3 mol d^{-1}; Table 3), which consequently appears to be related to pelagic production. Since dissolution also occurs in estuarine waters (accounting for 20-80% of pelagic $aSiO_2$ recycling; DeMaster et al., 1983; Ragueneau et al., 2002b; Beucher et al., 2004), it follows that other sources must also contribute to the deposition flux of $aSiO_2$. This exercise highlights the importance of directly quantifying the pelagic silica dissolution rates in estuaries to better constrain their budgets. In the Bay of Brest, pelagic dissolution rates were shown to recycle ~ 50% of $aSiO_2$ production annually (Beucher et al., 2004), but these rates could be even higher throughout estuaries because of enhanced $aSiO_2$ dissolution by bacterial degradation of organic coatings (Roubeix et al., 2008a).

As suggested in section 4.1., other possible sources of deposited $aSiO_2$ are benthic primary production, lateral resuspension and redistribution of particles from tidal mudflats and small water outlets. The high deposition fluxes of estuarine materials are particularly highlighted by benthic Chl *a* concentrations (140 $\mu g\ gDW^{-1}$; Figure 5B) that are much higher than those already reported in the Bay of Brest (Ragueneau et al., 1994; Sagan and Thouzeau, 1998; Ni Longphuirt et al., 2006). Such high Chl *a* (or fucoxantin) concentrations have previously been reported to mirror the higher pelagic and benthic production taken place in estuaries, the lateral resuspension and redistribution of particles, with the higher deposition rates related to a shallower water column (Sun et al., 1994; Mangalaa et al., 2017; Wallington et al., 2023). Marine loads might be low due to the absence of a connection between estuarine and coastal waters observed in the Elorn and Aulne estuaries (Savoye, 2001), except in the downstream parts of these estuaries where marine materials are more significant (Khalil et al., 2013). Marine $aSiO_2$ loads can however be much higher in some estuaries; for instance, it reaches 25% in the Scheldt estuary (Carbonnel et al., 2013).

The relative contribution of benthic $Si(OH)_4$ fluxes compared to river fluxes is consequently enhanced (Figure 8), which highlights the important role of benthic recycling to the pelagic ecosystem, especially in summer. Even if benthic fluxes are generally lower compared to river fluxes in large estuaries (Arndt et al., 2009), their contribution can become significant in small and shallow estuaries (Anderson, 1986), such as in the Elorn and Aulne, as well as during the low-flow season (this study). The contribution of benthic fluxes to the pelagic ecosystem in summer is higher in the Aulne than in the Elorn Estuary, not just due to the lower river flow, but also due to the higher benthic surface of the Aulne Estuary and its meandering shape (Raimonet et al., 2013a).

Finally, this work bring new data on Si retention in small macrotidal estuaries, at seasonal and annual scales. While retention is ≤ 5% of river Si flux in winter, it increases to 38% in summer, and even 67% when accounting for burial in intertidal mudflats (Table 3). The annual burial of Si in the Elorn and Aulne estuaries is estimated to be 7% in subtidal sediments, and 12% when accounting for intertidal mudflat burial. These estimates are similar for the two estuaries, but lower than a ten times bigger estuary, the Scheldt estuary, where annual retention of $Si(OH)_4$ and $aSiO_2$ are estimated to attain 28% and 64%, respectively (Carbonnel et al., 2013). Such difference is expected because of (1) higher water residence time in the Scheldt estuary, which increases retention and limits flushing, and (2) intense dredging activity, which reduce sediment export to the coastal zone (Carbonnel et al., 2013). In this study, we gathered and measured a large number of data to better constrain and limit uncertainties on our estimates. Our values could however be refined, e.g. by coupling our results with a hydro-sedimentary model e.g. Grasso et al. (2018) in order to quantify retention at a fine spatial and temporal scale. This could help in quantifying the spatial heterogeneity and the transient regime of erosion and export of estuarine sediments.

5 Conclusions

Diagenetic modeling accounting for two reactive $aSiO_2$ phases, as well as reprecipitation and bioirrigation processes, is a useful tool for determining benthic Si fluxes, e.g., deposition fluxes that are difficult to measure *in situ* in estuaries. The Elorn and Aulne tidal estuaries are characterized by high deposition and burial fluxes throughout the year, indicating the high potential retention in these estuaries. Benthic recycling increases from winter to summer. A representation of bioirrigation appears necessary in such bioirrigated estuarine sediments in order to account for the doubling of benthic fluxes at the sediment-water interface.

Reprecipitation is expected to be insignificant in the Elorn and Aulne estuaries, but this result should be confirmed through laboratory experiments. An investigation into the sediment dynamics in these estuaries and the importance of mudflats in estuarine retention would be of interest. In this study, the functioning of small and shallow tidal estuaries (Elorn and Aulne) is shown to be dominated by river inputs and export during high river flow conditions, and by estuarine internal recycling during summer. The application of a transport-reaction model accounting for benthic-pelagic coupling appears useful for quantifying the spatio-temporal variations of the benthic Si cycle (and carbon, nitrogen, and phosphorus cycles) along estuaries, and for investigating the impact of small scale variations (biological and physical processes) on the general functioning of the ecosystem.

Data availability statement

The raw data supporting the conclusions of this article will be made available by the authors upon request to interested researchers.

Ethics statement

The manuscript presents research on animals that do not require ethical approval for their study.

Author contributions

MR: Conceptualization, Data curation, Formal analysis, Investigation, Methodology, Project administration, Software, Validation, Visualization, Writing – original draft, Writing – review & editing. OR: Conceptualization, Funding acquisition, Investigation, Methodology, Project administration, Resources, Validation, Writing – review & editing. KS: Conceptualization, Resources, Writing – review & editing, Methodology, Software, Validation. KK: Writing – review & editing, Data curation. AL: Data curation, Writing – review & editing, Investigation, Methodology. EM: Data curation, Investigation, Methodology, Writing – review & editing. BM: Data curation, Investigation, Methodology, Writing – review & editing. CR: Investigation, Writing – review & editing. LM: Writing – review & editing, Conceptualization, Funding acquisition, Resources.

Funding

The author(s) declare financial support was received for the research, authorship, and/or publication of this article. This work was supported by the French National Program for Coastal Environment (PNEC-EC2CO), and the salaries of MR and EM were funded by the Ministère de l'Enseignement Supérieur et de la Recherche and the Conseil général du Finistère, respectively. Publication fees were partly funded by the Agence Nationale de la Recherche (ANR-23-CE03-0004-01).

Acknowledgments

We gratefully thank all the participants of the project, including the R/V *Côtes de la Manche* crew, Manon Le Goff, Bruno Bombled, Agnès Youenou, Françoise Andrieux-Loyer, Xavier Philippon, Florian Caradec for their valuable help for cores sampling and processing, Marie Czamanski, Solène Mineau, Tualenn Le Roch and Rudolph Corvaisier for their contribution to $aSiO_2$ measurements, Erwan Amice and Robert Marc for their helpfull assistance on board the *Hésione* (IUEM), Francois Maguer, Stéphane L'Helguen, Claire Labry, Daniel Delmas for surface water sampling, the ECOFLUX network (IUEM/Conseil Général du Finistère) for river flux data. For the purpose of Open Access, a CC-BY public copyright license has been applied by the authors to the present document and will be applied to all subsequent versions up to the Author Accepted Manuscript arising from this submission.

Conflict of interest

The authors declare that the research was conducted in the absence of any commercial or financial relationships that could be construed as a potential conflict of interest.

Publisher's note

References

Abbott, B. W., Moatar, F., Gauthier, O., Fovet, O., Antoine, V., and Ragueneau, O. (2018). Trends and seasonality of river nutrients in agricultural catchments: 18years of weekly citizen science in France. *Sci. Total Environ.* 624, 845–858. doi: 10.1016/j.scitotenv.2017.12.176

Aller, R. C., and Mackin, J. E. (1984). Preservation of reactive organic matter in marine sediments. *Earth Planetary Sci. Lett.* 70, 260–266. doi: 10.1016/0012-821X(84)90010-4

Anderson, G. F. (1986). Silica, diatoms and a freshwater productivity maximum in Atlantic Coastal Plain estuaries, Chesapeake Bay. *Estuarine Coast. Shelf Sci.* 22, 183–197. doi: 10.1016/0272-7714(86)90112-5

Andrieux-Loyer, F., Philippon, X., Bally, G., Kérouel, R., Youenou, A., and Le Grand, J. (2008). Phosphorus dynamics and bioavailability in sediments of the penzé Estuary (NW France): in relation to annual P-fluxes and occurrences of alexandrium minutum. *Biogeochemistry* 88, 213–231. doi: 10.1007/s10533-008-9199-2

Arndt, S., and Regnier, P. (2007). A model for the benthic-pelagic coupling of silica in estuarine ecosystems: sensitivity analysis and system scale simulation. *Biogeosciences* 4, 331–352. doi: 10.5194/bg-4-331-2007

Arndt, S., Regnier, P., and Vanderborght, J.-P. (2009). Seasonally-resolved nutrient export fluxes and filtering capacities in a macrotidal estuary. *J. Mar. Syst.* 78, 42–58. doi: 10.1016/j.jmarsys.2009.02.008

Arndt, S., Vanderborght, J.-P., and Regnier, P. (2007). Diatom growth response to physical forcing in a macrotidal estuary: Coupling hydrodynamics, sediment transport, and biogeochemistry. *J. Geophys. Res.: Oceans* 112. doi: 10.1029/2006JC003581

Bassoulet, P. (1979). *Etude de la dynamique des sédiments en suspension dans l'estuaire de l'Aulne (rade de Brest)*. (Brest, France: Université de Bretagne Occidentale).

Berner, R. A. (1980). *Early Diagenesis: A Theoretical Approach* (Princeton, New Jersey: Princeton University Press). doi: 10.1515/9780691209401

Beucher, C., Tréguer, P., Corvaisier, R., Hapette, A. M., and Elskens, M. (2004). Production and dissolution of biosilica, and changing microphytoplankton dominance in the Bay of Brest (France). *Mar. Ecol. Prog. Ser.* 267, 57–69. doi: 10.3354/meps267057

Boudreau, B. P. (1994). *Diagenetic models and their implementation. Modelling transport and reactions in aquatic sediments* (Berlin: Sringer).

Buesseler, K. O. (1998). The decoupling of production and particulate export in the surface ocean. *Global Biogeochemical Cycles* 12, 297–310. doi: 10.1029/97GB03366

Carbonnel, V., Lionard, M., Muylaert, K., and Chou, L. (2009). Dynamics of dissolved and biogenic silica in the freshwater reaches of a macrotidal estuary (The Scheldt, Belgium). *Biogeochemistry* 96, 49–72. doi: 10.1007/s10533-009-9344-6

Carbonnel, V., Vanderborght, J.-P., and Chou, L. (2013). *Silica Mass-Balance and Retention in the Riverine and Estuarine Scheldt Tidal System (Belgium/The Netherlands)*. Available at: http://agris.fao.org/agris-search/search.do?recordID=US201400145698 (Accessed December 23, 2016).

Carey, J. C., and Fulweiler, R. W. (2014). Salt marsh tidal exchange increases residence time of silica in estuaries. *Limnology Oceanography* 59, 1203–1212. doi: 10.4319/lo.2014.59.4.1203

Cariou-Le Gall, V., and Blanchard, G. F. (1995). Monthly HPLC measurements of pigment concentration from an intertidal muddy sediment of marennes-oléron bay, france. *Mar. Ecol. Prog. Ser.* 121, 171–179. doi: 10.3354/meps121171

Chauvaud, L., Jean, F., Ragueneau, O., and Thouzeau, G. (2000). Long-term variation of the bay of brest ecosystem: benthic-pelagic coupling revisited. *Mar. Ecol. Prog. Ser.* 200, 35–48. doi: 10.3354/meps200035

Cloern, J. E. (1982). Does the benthos control phytoplankton biomass in South San Francisco Bay? *Mar. Ecol. Prog. Ser.* 9, 191–202. doi: 10.3354/meps009191

Cloern, J. E., Jassby, A. D., Schraga, T. S., Nejad, E., and Martin, C. (2017). Ecosystem variability along the estuarine salinity gradient: Examples from long-term study of San Francisco Bay. *Limnology Oceanography* 62, S272–S291. doi: 10.1002/lno.10537

Conley, D. J. (1997). Riverine contribution of biogenic silica to the oceanic silica budget. *Limnology Oceanography* 42, 774–777. doi: 10.4319/lo.1997.42.4.0774

Conley, D. J., and Johnstone, R. (1995). Biogeochemistry of N, P and Si in Baltic Sea sediments: response to a simulated deposition of a spring diatom bloom. *Mar. Ecol. Prog. Ser.* 122, 265–276. doi: 10.3354/meps122265

Conley, D. J., Schelske, C. L., and Stoermer, E. F. (1993). Modification of the biogeochemical cycle of silica with eutrophication. *Mar. Ecol. Prog. Ser.* 101, 179–192. doi: 10.3354/meps101179

DeMaster, D. J. (1981). The supply and accumulation of silica in the marine environment. *Geochimica Cosmochimica Acta* 45, 1715–1732. doi: 10.1016/0016-7037(81)90006-5

DeMaster, D. J. (2002). The accumulation and cycling of biogenic silica in the Southern Ocean: revisiting the marine silica budget. *Deep Sea Res. Part II: Topical Stud. Oceanography* 49, 3155–3167. doi: 10.1016/S0967-0645(02)00076-0

DeMaster, D. J., Knapp, G. B., and Nittrouer, C. A. (1983). Biological uptake and accumulation of silica on the Amazon continental shelf. *Geochimica Cosmochimica Acta* 47, 1713–1723. doi: 10.1016/0016-7037(83)90021-2

DeMaster, D. J., McKee, B. A., Nittrouer, C. A., Jiangchu, Q., and Guodong, C. (1985). Rates of sediment accumulation and particle reworking based on radiochemical measurements from continental shelf deposits in the East China Sea. *Continental Shelf Res.* 4, 143–158. doi: 10.1016/0278-4343(85)90026-3

Dixit, S., Van Cappellen, P., and van Bennekom, A. J. (2001). Processes controlling solubility of biogenic silica and pore water build-up of silicic acid in marine sediments. *Mar. Chem.* 73, 333–352. doi: 10.1016/S0304-4203(00)00118-3

Duport, E., Stora, G., Tremblay, P., and Gilbert, F. (2006). Effects of population density on the sediment mixing induced by the gallery-diffusor Hediste (Nereis) diversicolor O.F. Mülle. *J. Exp. Mar. Biol. Ecol.* 336, 33–41. doi: 10.1016/j.jembe.2006.04.005

Dürr, H., Meybeck, M., Hartmann, J., Laruelle, G. g., and Roubeix, V. (2011). Global spatial distribution of natural riverine silica inputs to the coastal zone. *Biogeosciences* 8, 597–620. doi: 10.5194/bg-8-597-2011

Ehlert, C., Doering, K., Wallmann, K., Scholz, F., Sommer, S., Grasse, P., et al. (2016). Stable silicon isotope signatures of marine pore waters – Biogenic opal dissolution versus authigenic clay mineral formation. *Geochimica Cosmochimica Acta* 191, 102–117. doi: 10.1016/j.gca.2016.07.022

Emerson, S., Jahnke, R., and Heggie, D. (1984). Sediment-water exchange in shallow water estuarine sediments. *J. Mar. Res.* 42, 709–730. doi: 10.1357/002224084788505942

Eyre, B. D., and Ferguson, A. J. P. (2006). Impact of a flood event on benthic and pelagic coupling in a sub-tropical east Australian estuary (Brunswick). *Estuarine Coast. Shelf Sci.* 66, 111–122. doi: 10.1016/j.ecss.2005.08.008

Fabre, S., Jeandel, C., Zambardi, T., Roustan, M., and Almar, R. (2019). An overlooked silica source of the modern oceans: are sandy beaches the key? *Front. Earth Sci.* 7. doi: 10.3389/feart.2019.00231

Farmer, V. C., Delbos, E., and Miller, J. D. (2005). The role of phytolith formation and dissolution in controlling concentrations of silica in soil solutions and streams. *Geoderma* 127, 71–79. doi: 10.1016/j.geoderma.2004.11.014

Forja, J. M., and Gómez-Parra, A. (1998). Measuring nutrient fluxes across the sediment-water interface using benthic chambers. *Mar. Ecol. Prog. Ser.* 164, 95–105. doi: 10.3354/meps164095

François, F., Poggiale, J.-C., Durbec, J.-P., and Stora, G. (1997). A new approach for the modelling of sediment reworking induced by a macrobenthic community. *Acta Biotheoretica* 45, 295–319. doi: 10.1023/A:1000636109604

Fulweiler, R. W., and Nixon, S. W. (2009). "Responses of benthic-pelagic coupling to climate change in a temperate estuary," in *Eutrophication in Coastal Ecosystems: Towards better understanding and management strategies Selected Papers from the Second International Symposium on Research and Management of Eutrophication in Coastal Ecosystems, 20–23 June 2006, Nyborg, Denmark*. Eds. J. H. Andersen and D. J. Conley (Dordrecht: Springer Netherlands), 147–156. doi: 10.1007/978-90-481-3385-7_13

Gallinari, M., Ragueneau, O., DeMaster, D. J., Hartnett, H., Rickert, D., and Thomas, C. (2008). Influence of seasonal phytodetritus deposition on biogenic silica dissolution in marine sediments–potential effects on preservation. *Deep Sea Res. Part II: Topical Stud. Oceanography* 55, 2451–2464. doi: 10.1016/j.dsr2.2008.06.005

Garnier, J., Beusen, A., Thieu, V., Billen, G., and Bouwman, L. (2010). N:P:Si nutrient export ratios and ecological consequences in coastal seas evaluated by the ICEP approach. *Global Biogeochemical Cycles* 24, GB0A05. doi: 10.1029/2009GB003583

Garnier, J., Billen, G., Lassaletta, L., Vigiak, O., Nikolaidis, N. P., and Grizzetti, B. (2021). Hydromorphology of coastal zone and structure of watershed agro-food system are main determinants of coastal eutrophication. *Environ. Res. Lett.* 16, 023005. doi: 10.1088/1748-9326/abc777

Gehlen, M., and Van Raaphorst, W. (2002). The role of adsorption–desorption surface reactions in controlling interstitial Si(OH)4 concentrations and enhancing Si (OH)4 turn-over in shallow shelf seas. *Continental Shelf Res.* 22, 1529–1547. doi: 10.1016/S0278-4343(02)00016-X

Grasso, F., Verney, R., Le Hir, P., Thouvenin, B., Schulz, E., Kervella, Y., et al. (2018). Suspended sediment dynamics in the macrotidal seine estuary (France): 1. Numerical modeling of turbidity maximum dynamics. *J. Geophysical Research: Oceans* 123, 558–577. doi: 10.1002/2017JC013185

Green, M. A., Gulnick, J. D., Dowse, N., and Chapman, P. (2004). Spatiotemporal patterns of carbon remineralization and bio-irrigation in sediments of Casco Bay Estuary, Gulf of Maine. *Limnology Oceanography* 49, 396–407. doi: 10.4319/lo.2004.49.2.0396

Heip, C. H. R., Goosen, N. K., Herman, P. M. J., Kromkamp, J., Middelburg, J. J., and Soetaert, K. (1995). Production and consumption of biological particles in temperate tidal estuaries. In: *Oceanography and marine Biology: An Annual Review*. Available at: https://www.vliz.be/nl/open-marien-archief?module=ref&refid=8311&printversion=1&dropIMIStitle=1 (Accessed March 28, 2022).

Humborg, C., Ittekkot, V., Cociasu, A., and Bodungen, B. v (1997). Effect of Danube River dam on Black Sea biogeochemistry and ecosystem structure. *Nature* 386, 385–388. doi: 10.1038/386385a0

Kamatani, A. (1982). Dissolution rates of silica from diatoms decomposing at various temperatures. *Mar. Biol.* 68, 91–96. doi: 10.1007/BF00393146

Khalil, K., Laverman, A. M., Raimonet, M., and Rabouille, C. (2018). Importance of nitrate reduction in benthic carbon mineralization in two eutrophic estuaries: Modeling, observations and laboratory experiments. *Mar. Chem.* 199, 24–36. doi: 10.1016/j.marchem.2018.01.004

Khalil, K., Rabouille, C., Gallinari, M., Soetaert, K., Demaster, D. J., and Ragueneau, O. (2007). Constraining biogenic silica dissolution in marine sediments: A comparison between diagenetic models and experimental dissolution rates. *Mar. Chem.* 106, 223–238. doi: 10.1016/j.marchem.2006.12.004

Khalil, K., Raimonet, M., Laverman, A. M., Yan, C., Andrieux-Loyer, F., Viollier, E., et al. (2013). Spatial and temporal variability of sediment organic matter recycling in two temperate eutrophicated estuaries. *Aquat. Geochemistry* 19, 517–542. doi: 10.1007/s10498-013-9213-8

Laruelle, G. G. (2009). *Quantifying nutrient cycling and retention in coastal waters at the global scale*. Available at: http://dspace.library.uu.nl/handle/1874/35870 (Accessed January 2, 2017).

Le Bouteiller, A., Leynaert, A., Landry, M. R., Le Borgne, R., Neveux, J., Rodier, M., et al. (2003). Primary production, new production, and growth rate in the equatorial Pacific: Changes from mesotrophic to oligotrophic regime. *J. Geophys. Res.* 108. doi: 10.1029/2001JC000914

Lorenzen, C. J. (1966). A method for the continuous measurement of in *vivo* chlorophyll concentration. *Deep Sea Res. Oceanographic Abstracts* 13, 223–227. doi: 10.1016/0011-7471(66)91102-8

Loucaides, S., Michalopoulos, P., Presti, M., Koning, E., Behrends, T., and Van Cappellen, P. (2010). Seawater-mediated interactions between diatomaceous silica and terrigenous sediments: Results from long-term incubation experiments. *Chem. Geology* 270, 68–79. doi: 10.1016/j.chemgeo.2009.11.006

Maavara, T., Akbarzadeh, Z., and Van Cappellen, P. (2020). Global dam-driven changes to riverine N:P:Si ratios delivered to the coastal ocean. *Geophysical Res. Lett.* 47, e2020GL088288. doi: 10.1029/2020GL088288

Mangalaa, K. R., Cardinal, D., Brajard, J., Rao, D. B., Sarma, N. S., Djouraev, I., et al. (2017). Silicon cycle in Indian estuaries and its control by biogeochemical and anthropogenic processes. *Continental Shelf Res.* 148, 64–88. doi: 10.1016/j.csr.2017.08.011

Marinelli, R. L. (1992). Effects of polychaetes on silicate dynamics and fluxes in sediments: Importance of species, animal activity and polychaete effects on benthic diatoms. *J. Mar. Res.* 50, 745–779. doi: 10.1357/002224092784797566

McManus, J., Hammond, D. E., Berelson, W. M., Kilgore, T. E., Demaster, D. J., Ragueneau, O. G., et al. (1995). Early diagenesis of biogenic opal: Dissolution rates, kinetics, and paleoceanographic implications. *Deep Sea Res. Part II: Topical Stud. Oceanography* 42, 871–903. doi: 10.1016/0967-0645(95)00035-O

Michalopoulos, P., and Aller, R. C. (2004). Early diagenesis of biogenic silica in the Amazon delta: alteration, authigenic clay formation, and storage. *Geochimica Cosmochimica Acta* 68, 1061–1085. doi: 10.1016/j.gca.2003.07.018

Michaud, E. (2006). *Rôle de la diversité fonctionnelle de la communauté à macoma balthica (Estuaire du saint-laurent, québec, canada) sur les flux biogéochimiques à l'interface eau-sèdiment et sur le mélange particulaire*. Available at: http://www.theses.fr/2006AIX22056.

Moriceau, B., Goutx, M., Guigue, C., Lee, C., Armstrong, R., Duflos, M., et al. (2009). Si–C interactions during degradation of the diatom Skeletonema marinoi. *Deep Sea Res. Part II: Topical Stud. Oceanography* 56, 1381–1395. doi: 10.1016/j.dsr2.2008.11.026

Nelson, D. M., Tréguer, P., Brzezinski, M. A., Leynaert, A., and Quéguiner, B. (1995). Production and dissolution of biogenic silica in the ocean: Revised global estimates, comparison with regional data and relationship to biogenic sedimentation. *Global Biogeochemical Cycles* 9, 359–372. doi: 10.1029/95GB01070

Nelson, J. R. (1993). Rates and possible mechanism of light-dependent degradation of pigments in detritus derived from phytoplankton. *J. Mar. Res.* 51, 155–179. doi: 10.1357/0022240933223837

Nichols, F. H., Cloern, J. E., Luoma, S. N., and Peterson, D. H. (1986). The modification of an estuary. *Science* 231, 567–573. doi: 10.1126/science.231.4738.567

Ni Longphuirt, S. N., Leynaert, A., Guarini, J., Chauvaud, L., Claquin, P., Herlory, O., et al. (2006). Discovery of microphytobenthos migration in the subtidal zone. *Mar. Ecol. Prog. Ser.* 328, 143–154. doi: 10.3354/meps328143

Officer, C. B., and Ryther, J. H. (1980). The possible importance of silicon in marine eutrophication. *Mar. Ecol. Prog. Ser.* 3, 83–91. doi: 10.3354/meps003083

Oleszczuk, B., Michaud, E., Morata, N., Renaud, P. E., and Kędra, M. (2019). Benthic macrofaunal bioturbation activities from shelf to deep basin in spring to summer transition in the Arctic Ocean. *Mar. Environ. Res.* 150, 104746. doi: 10.1016/j.marenvres.2019.06.008

Peterson, D. H. (1979). Sources and sinks of biologically reactive oxygen, carbon, nitrogen, and silica in northern San Francisco Bay. *Estuar. Res.*, 153–187.

Pondaven, P., Ragueneau, O., Tréguer, P., Hauvespre, A., Dezileau, L., and Reyss, J. L. (2000). Resolving the 'opal paradox' in the southern ocean. *Nature* 405, 168–172. doi: 10.1038/35012046

Presti, M., and Michalopoulos, P. (2008). Estimating the contribution of the authigenic mineral component to the long-term reactive silica accumulation on the western shelf of the Mississippi River Delta. *Continental Shelf Res.* 28, 823–838. doi: 10.1016/j.csr.2007.12.015

Pritchard, D. W. (1967). *What is an estuary: Physical Viewpoint* (American Association for the Advancement of Science). Available at: https://tamug-ir.tdl.org/handle/1969.3/24383 (Accessed March 29, 2022).

Querné, J. (2011). *Invasion de Spartina alterniflora dans les marais de la rade de Brest. Comportement invasif et impact sur le cycle biog\textbackslash'eochimique du silicium*. Available at: http://scholar.google.fr/scholar?q=related:OBhHKBbubiUJ:scholar.google.com/&hl=fr&as_sdt=0,5 (Accessed May 8, 2012).

Ragueneau, O., Chauvaud, L., Leynaert, A., Thouzeau, G., Paulet, Y.-M., Bonnet, S., et al. (2002a). Direct evidence of a biologically active coastal silicate pump: Ecological implications. *Limnology Oceanography* 47, 1849–1854. doi: 10.4319/lo.2002.47.6.1849

Ragueneau, O., Chauvaud, L., Moriceau, B., Leynaert, A., Thouzeau, G., Donval, A., et al. (2005a). Biodeposition by an Invasive suspension feeder impacts the biogeochemical cycle of si in a coastal ecosystem (Bay of brest, France). *Biogeochemistry* 75, 19–41. doi: 10.1007/s10533-004-5677-3

Ragueneau, O., Conley, D. J., DeMaster, D. J., Dürr, H. H., and Dittert, N. (2010). Biogeochemical Transformations of Silicon Along the Land–Ocean Continuum and Implications for the Global Carbon Cycle1. In: *Carbon and nutrient fluxes in continental margins* (Springer). Available at: http://link.springer.com/chapter/10.1007/978-3-540-92735-8_10 (Accessed April 10, 2015).

Ragueneau, O., De Blas Varela, E., Tréguer, P., Quéguiner, B., and Del Amo, Y. (1994). Phytoplankton dynamics in relation to the biogeochemical cycle of silicon in a coastal ecosystem of western Europe. *Mar. Ecol. Prog. Ser.* 106, 157–172. doi: 10.3354/meps106157

Ragueneau, O., Lancelot, C., Egorov, V., Vervlimmeren, J., Cociasu, A., Déliat, G., et al. (2002b). Biogeochemical transformations of inorganic nutrients in the mixing zone between the danube river and the North-western Black Sea. *Estuarine Coast. Shelf Sci.* 54, 321–336. doi: 10.1006/ecss.2000.0650

Ragueneau, O., Savoye, N., Del Amo, Y., Cotten, J., Tardiveau, B., and Leynaert, A. (2005b). A new method for the measurement of biogenic silica in suspended matter of coastal waters: using Si:Al ratios to correct for the mineral interference. *Continental Shelf Res.* 25, 697–710. doi: 10.1016/j.csr.2004.09.017

Ragueneau, O., Schultes, S., Bidle, K., Claquin, P., and Moriceau, B. (2006). Si and C interactions in the world ocean: Importance of ecological processes and implications for the role of diatoms in the biological pump. *Global Biogeochemical Cycles* 20. doi: 10.1029/2006GB002688

Ragueneau, O., and Tréguer, P. (1994). Determination of biogenic silica in coastal waters: applicability and limits of the alkaline digestion method. *Mar. Chem.* 45, 43–51. doi: 10.1016/0304-4203(94)90090-6

Raimonet, M., Andrieux-Loyer, F., Ragueneau, O., Michaud, E., Kérouel, R., Philippon, X., et al. (2013a). Strong gradient of benthic biogeochemical processes along a macrotidal temperate estuary: focus on P and Si cycles. *Biogeochemistry* 10. doi: 10.1007/s10533-013-9843-3

Raimonet, M., Ragueneau, O., Andrieux-Loyer, F., Philippon, X., Kerouel, R., Le Goff, M., et al. (2013b). Spatio-temporal variability in benthic silica cycling in two macrotidal estuaries: Causes and consequences for local to global studies. *Estuarine Coast. Shelf Sci.* 119, 31–43. doi: 10.1016/j.ecss.2012.12.008

Raimonet, M., Ragueneau, O., Jacques, V., Corvaisier, R., Moriceau, B., Khripounoff, A., et al. (2015). Rapid transport and high accumulation of amorphous silica in the Congo deep-sea fan: A preliminary budget. *J. Mar. Syst.* 141, 71–79. doi: 10.1016/j.jmarsys.2014.07.010

Rebreanu, L. (2009). *Study of the Si biogeochemical cycle in the sediments of the Scheldt continuum, Belgium/The Netherlands*. Available at: http://hdl.handle.net/2013/ (Accessed March 28, 2022).

Regnier, P., Friedlingstein, P., Ciais, P., Mackenzie, F. T., Gruber, N., Janssens, I. A., et al. (2013). Anthropogenic perturbation of the carbon fluxes from land to ocean. *Nat. Geosci.* 6, 597–607. doi: 10.1038/ngeo1830

Regnier, P., Mouchet, A., Wollast, R., and Ronday, F. (1998). A discussion of methods for estimating residual fluxes in strong tidal estuaries. *Continental Shelf Res.* 18, 1543–1571. doi: 10.1016/S0278-4343(98)00071-5

Riaux-Gobin, C., and Klein, B. (1993). "Microphytobenthic Biomass Measurement Using HPLC and Conventional Pigment Analysis," in *Handbook of Methods in Aquatic Microbial Ecology* (Boca Raton, London, New York, Washington DC: CRC Press).

Ridd, P., Day, G., Thomas, S., Harradence, J., Fox, D., Bunt, J., et al. (2001). Measurement of Sediment deposition rates using an optical backscatter sensor. *Estuarine Coast. Shelf Sci.* 52, 155–163. doi: 10.1006/ecss.2000.0635

Roubeix, V., Becquevort, S., and Lancelot, C. (2008a). Influence of bacteria and salinity on diatom biogenic silica dissolution in estuarine systems. *Biogeochemistry* 88, 47–62. doi: 10.1007/s10533-008-9193-8

Roubeix, V., Rousseau, V., and Lancelot, C. (2008b). Diatom succession and silicon removal from freshwater in estuarine mixing zones: From experiment to modelling. *Estuarine Coast. Shelf Sci.* 78, 14–26. doi: 10.1016/j.ecss.2007.11.007

Sagan, G., and Thouzeau, G. (1998). Microphytobenthic biomass in the Bay of Brest and the western English Channel. *Oceanologica Acta* 5, 677–694. doi: 10.1016/S0399-1784(99)80024-3

Savoye, N. (2001). *Origine et transfert de la matière organique particulaire dans les écosystèmes littoraux macrotidaux*. (Brest, France: Université de Bretagne Occidentale).

Shiller, A. M. (1996). The effect of recycling traps and upwelling on estuarine chemical flux estimates. *Geochimica Cosmochimica Acta* 60, 3177–3185. doi: 10.1016/0016-7037(96)00159-7

Smis, A., Van Damme, S., Struyf, E., Clymans, W., Van Wesemael, B., Frot, E., et al. (2011). A trade-off between dissolved and amorphous silica transport during peak flow events (Scheldt river basin, Belgium): impacts of precipitation intensity on terrestrial Si dynamics in strongly cultivated catchments. *Biogeochemistry* 106, 475–487. doi: 10.1007/s10533-010-9527-1

Soetaert, K. (2009). *rootSolve: Nonlinear root finding, equilibrium and steady-state analysis of ordinary differential equations*. Available at: https://cran.r-project.org/package=rootSolve.

Soetaert, K., and Petzoldt, T. (2010). Inverse modelling, sensitivity and monte carlo analysis in r using package FME. *J. Stat. Softw.* 33, 1–28. doi: 10.18637/jss.v033.i03

Soetaert, K., Middelburg, J. J., Heip, C., Meire, P., Van Damme, S., and Maris, T. (2006). Long-term change in dissolved inorganic nutrients in the heterotrophic Scheldt estuary (Belgium, The Netherlands). *Limnology Oceanography* 51, 409–423. doi: 10.4319/lo.2006.51.1_part_2.0409

Struyf, E., Dausse, A., Van Damme, S., Bal, K., Gribsholt, B., Boschker, H. T. S., et al. (2006). Tidal marshes and biogenic silica recycling at the land-sea interface. *Limnology Oceanography* 51, 838–846. doi: 10.4319/lo.2006.51.2.0838

Sun, M.-Y., Aller, R. C., and Lee, C. (1994). Spatial and temporal distributions of sedimentary chloropigments as indicators of benthic processes in Long Island Sound. *J. Mar. Res.* 52, 149–176. doi: 10.1357/0022240943076768

Sun, M.-Y., Lee, C., and Aller, R. C. (1993). Anoxic and oxic degradation of 14C-labeled chloropigments and a 14C-labeled diatom in long island sound sediments. *Limnology Oceanography* 38, 1438–1451. doi: 10.4319/lo.1993.38.7.1438

Sundbäck, K., Miles, A., Hulth, S., Pihl, L., Engström, P., Selander, E., et al. (2003). Importance of benthic nutrient regeneration during initiation of macroalgal blooms in shallow bays. *Mar. Ecol. Prog. Ser.* 246, 115–126. doi: 10.3354/meps246115

Tatters, A. O., Fu, F.-X., and Hutchins, D. A. (2012). High CO2 and silicate limitation synergistically increase the toxicity of pseudo-nitzschia fraudulenta. *PloS One* 7, e32116. doi: 10.1371/journal.pone.0032116

Testa, J. M., and Kemp, W. M. (2008). Variability of biogeochemical processes and physical transport in a partially stratified estuary: a box-modeling analysis. *Mar. Ecol. Prog. Ser.* 356, 63–79. doi: 10.3354/meps07264

Tréguer, P. (2002). Silica and the cycle of carbon in the ocean. *Comptes Rendus Geosci.* 334, 3–11. doi: 10.1016/S1631-0713(02)01680-2

Tréguer, P., Bowler, C., Moriceau, B., Dutkiewicz, S., Gehlen, M., Aumont, O., et al. (2018). Influence of diatom diversity on the ocean biological carbon pump. *Nat. Geosci.* 11, 27–37. doi: 10.1038/s41561-017-0028-x

Tréguer, P., and Le Corre, P. (1975). *Manuel d'analyse des sels nutritifs dans l'eau de mer: utilisation de l'auto-analyseur Technicon II* (Rapport de l'Universite de Bretagne Occidentale, Brest). Available at: https://ci.nii.ac.jp/naid/10012431976/ (Accessed March 28, 2022).

Tréguer, P. J., Sutton, J. N., Brzezinski, M., Charette, M. A., Devries, T., Dutkiewicz, S., et al. (2021). Reviews and syntheses: The biogeochemical cycle of silicon in the modern ocean. *Biogeosciences* 18, 1269–1289. doi: 10.5194/bg-18-1269-2021

Van Cappellen, P., Dixit, S., and van Beusekom, J. (2002). Biogenic silica dissolution in the oceans: Reconciling experimental and field-based dissolution rates. *Global Biogeochemical Cycles* 16, 1075. doi: 10.1029/2001GB001431

Wallington, H., Hendry, K., Perkins, R., Yallop, M., and Arndt, S. (2023). Benthic diatoms modify riverine silicon export to a marine zone in a hypertidal estuarine environment. *Biogeochemistry* 162, 177–200. doi: 10.1007/s10533-022-00997-7

Ward, J. P., Hendry, K. R., Arndt, S., Faust, J. C., Freitas, F. S., Henley, S. F., et al. (2022). Benthic silicon cycling in the Arctic Barents Sea: a reaction–transport model study. *Biogeosciences* 19, 3445–3467. doi: 10.5194/bg-19-3445-2022

Welsby, H. J., Hendry, K. R., and Perkins, R. G. (2016). The role of benthic biofilm production in the mediation of silicon cycling in the Severn Estuary, UK. *Estuarine Coast. Shelf Sci.* 176, 124–134. doi: 10.1016/j.ecss.2016.04.008

Yamada, S. S., and D'Elia, C. F. (1984). Silicic acid regeneration from estuarine sediment cores. *Mar. Ecol. Prog. Ser.* 18, 113–118. doi: 10.3354/meps018113

Zhang, Z., Cao, Z., Grasse, P., Dai, M., Gao, L., Kuhnert, H., et al. (2020). Dissolved silicon isotope dynamics in large river estuaries. *Geochimica Cosmochimica Acta* 273, 367–382. doi: 10.1016/j.gca.2020.01.028